Science of the Total Environment 959 (2025) 178261

Contents lists available at ScienceDirect

Science of the Total Environment

journal homepage: www.elsevier.com/locate/scitotenv

Warmer air temperatures predicted to result in wetland drying in the Upper Columbia River Valley, British Columbia, Canada

Italo Sampaio Rodrigues [a,*], Christopher Hopkinson [a], Laura Chasmer [a], Ryan J. MacDonald [a], Suzanne E. Bayley [b]

[a] Department of Geography and Environment, University of Lethbridge, Canada
[b] Department of Biological Sciences, University of Alberta, Canada

HIGHLIGHTS

- ANN-predicted seasonal land cover from historical Landsat time series.
- Hydroclimatic models (air temperature and precipitation) to predict river discharge.
- The open water area decreased while woody vegetation expanded.
- Peak river discharge and open water area projected in the spring.
- ANN projected late summer open water decline, similar to hydroclimatic projections.

GRAPHICAL ABSTRACT

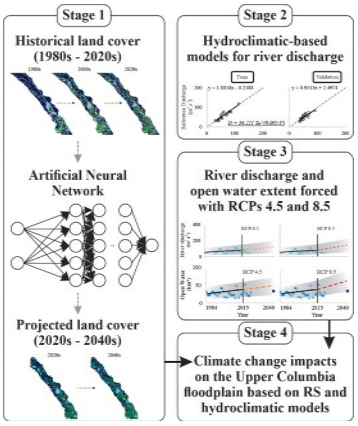

ARTICLE INFO

Editor: Gwenaël Imfeld

Keywords:
Ecohydrology
Remote sensing
Machine learning
Climate change
Montane ecosystems

ABSTRACT

Climatic warming is likely to affect the Canadian Rockies, leading to changes in the land cover (LC) and hydrological cycles. This study estimates climate-induced changes in LC (open water, marsh, wet meadow, and woody/shrub) in the Upper Columbia River Wetlands (UCRW), British Columbia, Canada, from 1984 to 2040. An artificial Neural Network (ANN) approach was used with Landsat series archive data from 1984 to 2022 to project seasonal LC change from 2020s to 2040s. Concurrently, hydroclimatic-based models (using air temperature and precipitation to predict river discharge at the UCRW, 1984–2022) were developed (average Nash Sutcliffe: training 0.75 and validation of 0.70) to predict (1984–2040) river discharge forced by Representative Concentration Pathway (RCP) 4.5 and 8.5. The 1984–2022 regression between river discharge and UCRW open water area was forced by RCP scenario river discharge results, calculating open water area for both scenarios. ANN-predicted LC with a Kappa of 0.85 (average of all seasons) for 2020s reference and projected LC, and 0.82 for reference and projected LC change maps (2000s–2020s). From 2020s to 2040s, the ANN projected a reduction (−5 %) of open water areas during late summer (August to mid-September) in the UCRW, consistent with RCP 4.5 forecasts. The peak of the open water area in the UCRW is projected to shift from summer (late-May to July)

* Corresponding author.
E-mail address: italo.rodrigues@uleth.ca (I.S. Rodrigues).

https://doi.org/10.1016/j.scitotenv.2024.178261
Received 16 October 2024; Received in revised form 19 December 2024; Accepted 21 December 2024
Available online 28 December 2024

to spring (April to mid-May) in both RCP scenarios. The projected changing hydrological conditions reduced the marsh area (−1 % to −12 %) and increased the wet meadow (+1 % to +4 %) mostly in the summer and late summer. Meanwhile, woody and shrubby vegetation on the floodplain increased (3 % to 5 %), indicating that the floodplain is projected to dry out.

1. Introduction

Montane wetlands act as sentinels of environmental change (Williamson et al., 2008; Moser et al., 2019) because they experience a significant elevational gradient where isotherms change quickly in space and time, altering seasonal freeze–thaw cycles (Edwards et al., 2008; Löffler et al., 2011), precipitation/runoff (Stewart, 2009), and therefore, vegetation change (Hrach et al., 2022). Montane wetlands also influence downstream hydrology and ecology (Chatterjee et al., 2010) by storing water during wet periods and supplying downstream flows during dry periods (Brinson and Malvárez, 2002). They also provide critical habitats for local biota (Cooper et al., 2017), provide support for food chains (Díaz et al., 2014), filter and store sediment and nutrients from runoff erosion events (Lottig et al., 2013), and store and emit carbon (Hrach et al., 2022).

Climate-mediated changes in hydrology have had numerous ecological implications in montane wetlands. For example, satellite time-series data over the Upper Colombia River Wetlands (UCRW) showed that open water extent decreased (1984 to 2022), and the encroachment of woody vegetation increased across the floodplain (Rodrigues et al., 2024). In the Rocky Mountains of Alberta, Glines (2012) documented a positive woody and shrub trend of 0.9 % cover year^{-1} from 1952 to 2003. A positive woody and shrub encroachment trend of 0.2 % cover year^{-1} over 62 years was also reported by Formica et al. (2014) in Niwot Ridge, south of the Rocky Mountains. Woody vegetation expansion influences hydrology (DeBeer et al., 2021; Leipe and Carey, 2021) by increasing canopy interception (Zwieback et al., 2019), evapotranspiration (Aguirre et al., 2020), and water infiltration (VanShaar et al., 2002).

Higher air temperatures are predicted over the Columbia River headwaters in the future (Flannigan et al., 2009; Schnorbus et al., 2012; Carver, 2017; Wang et al., 2017), which is expected to increase rates of snow and glacier melt (Moore et al., 2020), annual river flow, and lake size (Johnson et al., 2005). During late summer, glacier melt can increase river discharge and connected wetland area (e.g., open water) (Stahl and Moore, 2006; Jost et al., 2012). However, climate change-driven glacier melt in western Canada may disrupt local wetland hydrology and dependent biota since they will no longer supply water for

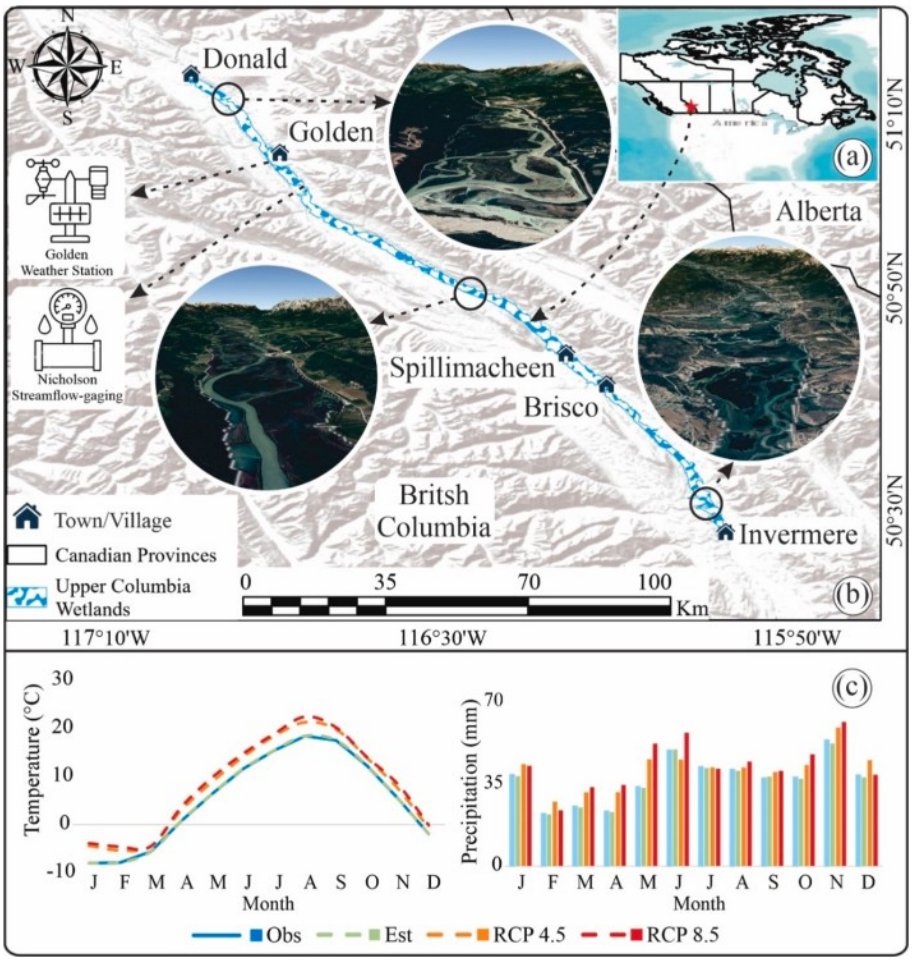

Fig. 1. a) The study location in Canada; b) Upper Columbia River Wetlands study area; c) observed, estimated and predicted meteorological data for Golden, BC where, Obs — Historical monthly averages at Golden meteorological station (1984 to 2022); Est — Estimated Historical monthly averages with bias correction by CanESM5 (1984 to 2014); RCP 4.5 — Projected (2015 to 2040) monthly averages with bias correction (Linear Scaling Method — LSM) by CanESM5 under RCP 4.5; RCP 8.5 — Projected (2015 to 2040) monthly averages with bias correction (LSM) by CanESM-2 under RCP 8.5.

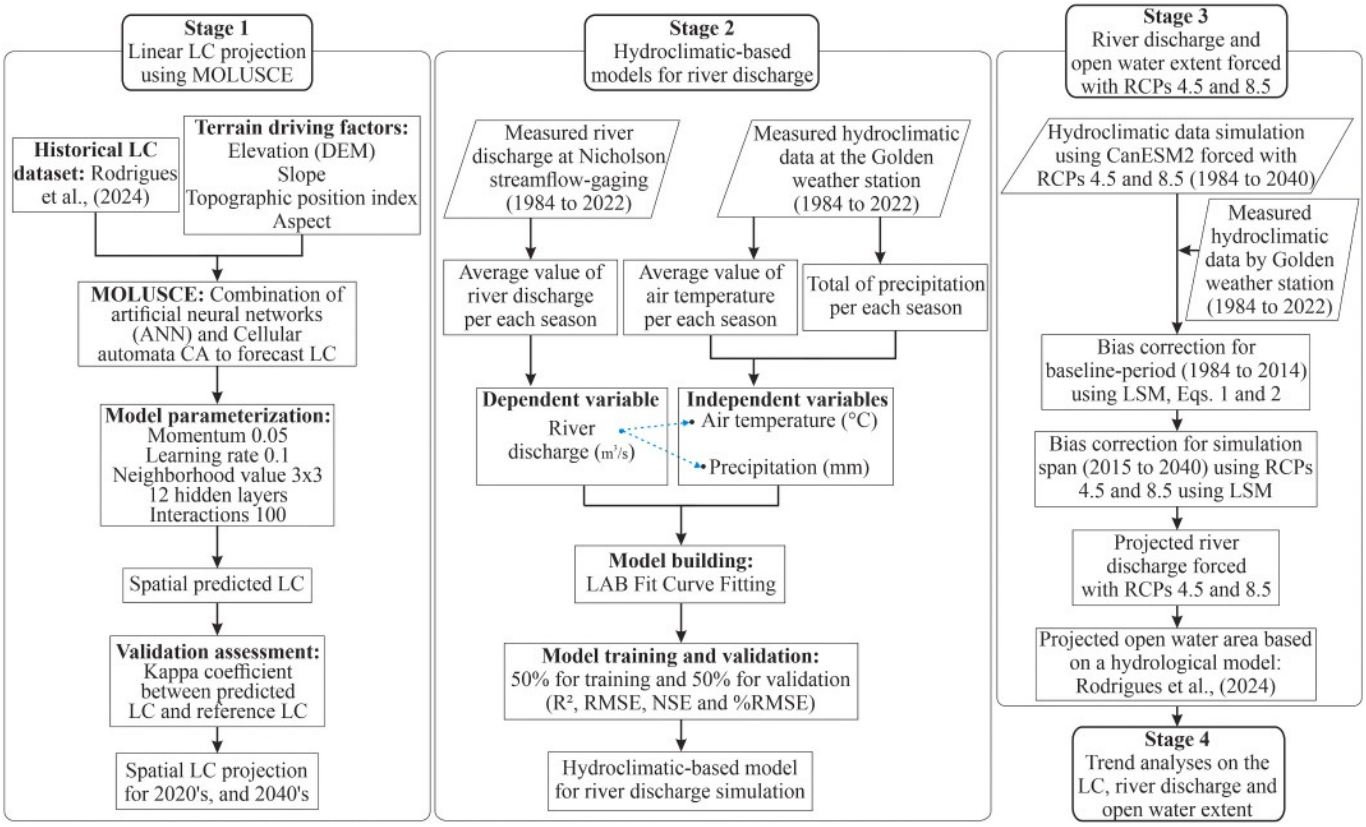

Fig. 2. Methodological flowchart for assessing climate change impacts in the LC and river discharge in the UCRW.

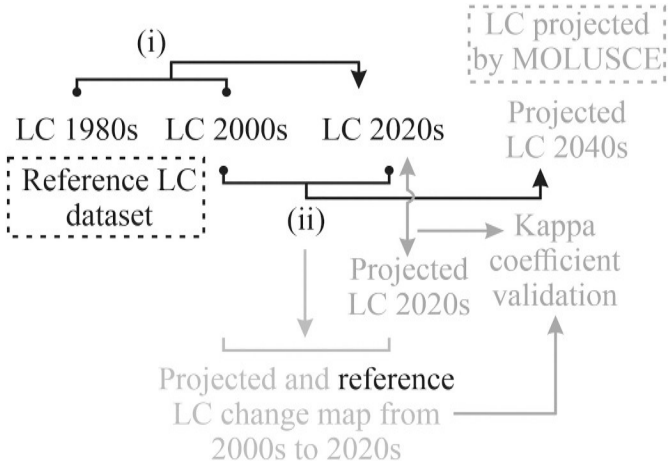

Fig. 3. LC forecast approach using MOLUSCE (i and ii: the steps and datasets used to project LC over the future).

this environment in the future (Clarke et al., 2015; Tsuruta and Schnorbus, 2021). Furthermore, the anticipated increase in evapotranspiration during late summer due to atmospheric warming (Moore et al., 2008) is expected to elevate the risk of drought (Harrington and Flannigan, 1993; Girardin et al., 2006; Kienzle, 2006; Wang et al., 2020). Consequently, there is uncertainty regarding the future of these wetlands and whether the associated ecosystems can be sustained under a changing climate regime.

The process of projecting the climate response of a watershed frequently involves the use of a hydrological model forced by climate scenarios (Tsuruta and Schnorbus, 2021). Since the 2014 IPCC Fifth Assessment Report, greenhouse gas concentration scenarios are based on Representative Concentration Pathways (RCP), which express atmospheric radiative forcing associated with different greenhouse gas emission scenarios predicted to 2100. Frequently used scenarios for climate change studies are RCP 4.5 (business-as-usual emissions; radiative forcing reaches 4.5 W m^{-2} by 2050, stabilizing early after 2100 (Thomson et al., 2011)) and RCP 8.5 (extreme baseline emissions, radiative forcing grows to 8.5 W m^{-2} by 2100 (Bjørnæs, 2013)).

Another method of examining the effects of climate change is to project land cover (LC) and river discharge (Gomes et al., 2020; Tsuruta and Schnorbus, 2021). Remote sensing (RS) is an effective tool to detect LC changes (e.g. there is at least 40 years of satellite imagery data using the moderate resolution satellite series: Landsat) (Amani et al., 2021; Wulder et al., 2022). Historical LC data can be utilized to project future LC by using the Artificial Neural Networks (ANN) approach (Rahman et al., 2017; Kamaraj and Rangarajan, 2022). The spatial visualization of the projected LC allows decision-makers to act in these specific vulnerable locations that are expected to change over time. Alternatively, empirical hydroclimatic-based models driven by air temperature and precipitation can be used to simulate the past and project the future of river discharge (Zhang et al., 2011; Diomede et al., 2008).

In this context, hydroclimatic-based models forced by RCM data can be used to project the river discharge in different RCP scenarios. Also, the integration of ANN with RS data (particularly the Landsat time-series) can aid in the prediction of spatial wetland trends and changes. Both approaches enable an evaluation of past and potential future trends across vast areas, thereby facilitating a deeper understanding of changes in montane wetland ecosystems.

This research aimed to forecast and describe the effects of climate change on Open Water, Marsh, Wet Meadow, and Woody/Shrub LCs in the Upper Columbia River Wetlands (UCRW) in British Columbia (BC), Canada using Landsat image archive time series and hydroclimatic models. The specific objectives are (i) to linearly project observed historical LC changes into the future up to 2040s; (ii) to compare/verify the

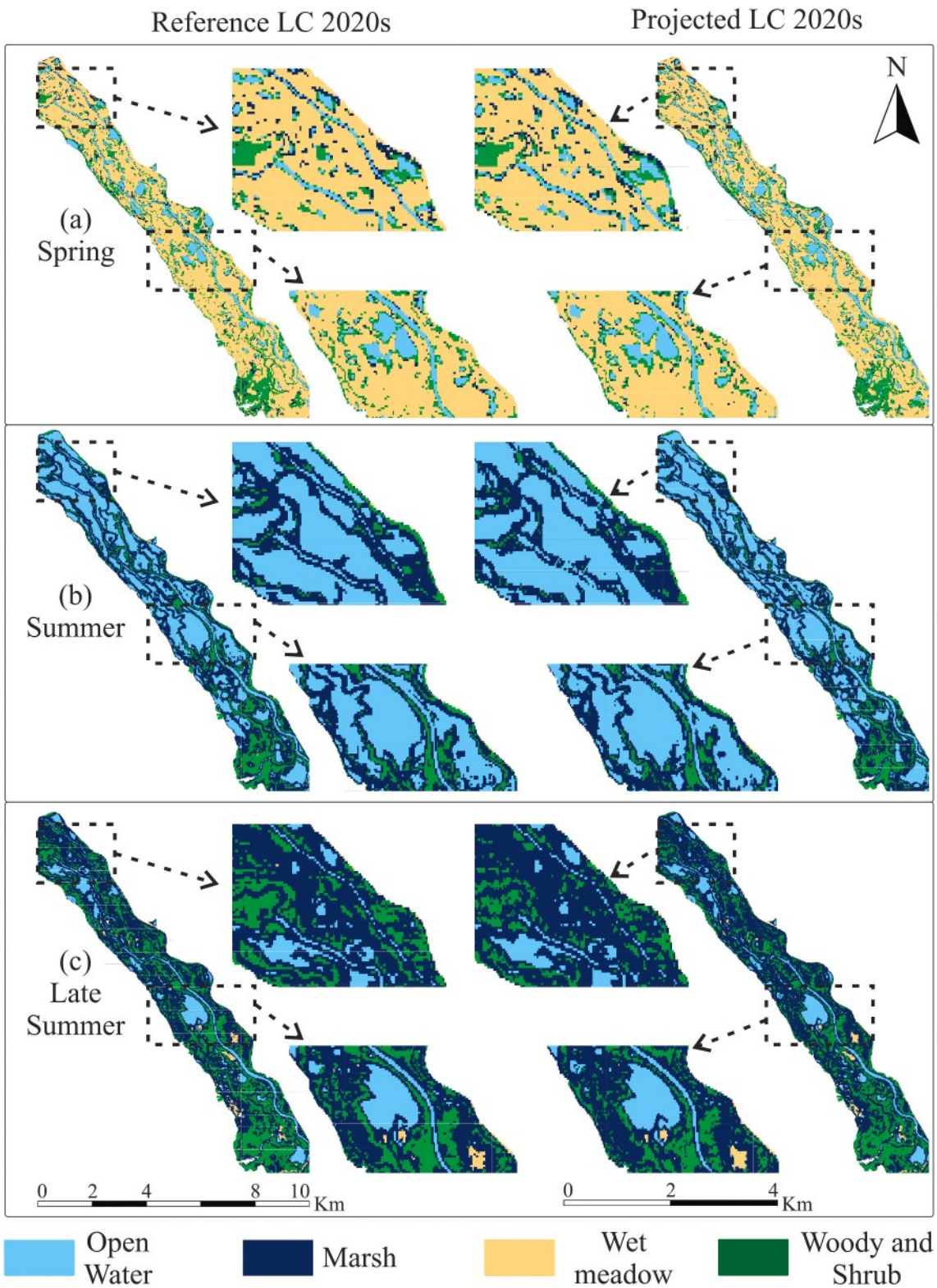

Fig. 4. Comparison of central section (portion of Spillimacheen to Golden, spanning an ~14 km stretch) of the UCRW reference and projected LC for 2020's during the spring (a), summer (b), and late summer (c).

projected open water LC by independently modelling the discharge and open water extents using RCP 4.5; (iii) to quantify and evaluate the projected trends and changes in areal floodplain land cover extents within the UCRW. Meanwhile, RCP 8.5 provides an upper estimate of wetland changes. Outputs of the research will assist in the strategic planning and management of local wetlands in the Columbia Valley for future water and habitat management by developing a methodology to assess the possible effects of future climate change on montane floodplain landscapes.

Table 1
Confusion matrix with commission and omission errors between the reference and projected land cover change of 2020's during spring (i.e., April to mid-May).

Classes	OW-M	OW-WM	OW-WS	M-OW	M-WM	M-WS	WM-OW	WM-M	WM-WS	WS-OW	WS-M	WS-WM	Marginal total	Comission error	Total accuracy	Kappa index
OW-M	74	2	2	4	2	4	2	1	2	2	3	2	100	0.26	79.9 %	0.78
OW-WM	3	74	1	3	4	3	1	3	2	1	3	2	100	0.26		
OW-WS	2	0	80	3	4	3	3	1	1	0	2	1	100	0.20		
M-OW	2	3	1	76	1	3	3	2	2	3	3	1	100	0.24		
M-WM	1	3	2	3	80	3	5	2	1	0	0	0	100	0.20		
M-WS	2	2	2	1	1	79	2	2	3	2	2	2	100	0.21		
WM-OW	0	2	1	1	3	0	80	2	3	3	3	2	100	0.20		
WM-M	1	2	2	2	1	1	2	80	2	2	3	2	100	0.20		
WM-WS	2	2	3	2	2	2	1	2	79	2	1	2	100	0.21		
WS-OW	0	0	2	1	1	2	0	2	2	84	3	3	100	0.16		
WS-M	0	1	2	1	1	2	1	3	1	2	86	0	100	0.14		
WS-WM	0	1	2	2	3	1	0	0	1	2	1	87	100	0.13		
Marginal total	87	92	100	99	103	103	100	100	99	103	110	104	1200			
Omission error	0.15	0.20	0.20	0.23	0.22	0.23	0.20	0.20	0.20	0.18	0.22	0.16				

1) OW-M: open water to marsh; 2) OW-WM: open water to wet meadow; 3) OW-WS: open water to woody/shrub; 4) M-OW: marsh to open water; 5) M-WM: marsh to wet meadow; 6) M-WS: marsh to woody/shrub; 7) WM-OW: wet meadow to open water; 8) WM-M: wet meadow to marsh; 9) WM-WS: wet meadow to woody/shrub; 10) WS-OW: woody/shrub to open water; 11) WS-M: woody/shrub to marsh; and 12) WS-WM: woody/shrub to wet meadow.

2. Materials and methods

2.1. Study area

The Upper Columbia River Wetlands are in Southeastern British Columbia, Canada, spanning an ~120 km stretch of the Columbia River floodplain (188 km^2) between the towns of Donald and Invermere (Fig. 1). The open-water areas of these floodplain wetlands are distinguished by collections of emergent and submerged aquatic plants (Marsh and Wet meadow), which provide essential habitat and other resources for fish, invertebrates, amphibians, and birds (Rooney et al., 2013). The study area has a humid continental mild summer climate (Köppen climate classification), with cold winters, and short, cool summers. For Golden, B.C., the mean annual average air temperature is 3 °C, and total precipitation ~800 mm $year^{-1}$ (Environment Canada, 2022a). The annual average peak river flow at Nicholson, upstream of Golden, is 512 $m^3\ s^{-1}$ (Carli and Bayley, 2015). Annual air temperature is predicted to increase by 0.02 and 0.03 °C $year^{-1}$ by 2040 based on RCP 4.5 and 8.5 scenarios (Swart et al., 2019; ECCC, 2021) (Fig. 1c — see below).

2.2. Data

The historical (1984–2022) river discharge data were acquired from the Nicholson gauge (Environment Canada, 2022b; Columbia River at Nicholson, 08NA002; Location: 51° 14′ 36″ N, 116° 54′ 46″ W). Historical (1984–2022) air temperature (T_{air}) and precipitation (P), data were obtained from the Golden Weather station (Environment Canada, 2022a; Golden A, 1173209; Location: 51° 17′ 57″ N, 116° 58′ 56″ W). This station was chosen due to its extensive historical record and its location within the main valley of the study area.

The projected daily T_{air} and P were obtained from a subset of the Canadian CanESM5 model (Swart et al., 2019), which is part of the Coupled Model Intercomparison Project Phase 6 (CMIP6) global climate models (GCMs) (Environment and Climate Change Canada, 2021). The grids were established with a longitude and latitude of 2.8125°, which corresponds to a spatial resolution of ~312 km. Outputs from GCMs are subject to systematic scale-based deviations from location-specific values, therefore, bias-correction is recommended to ensure simulation reliability (Teutschbein and Seibert, 2012). The Linear Scaling Method (LSM) was used to correct bias, as this method has proven effective for bias-correction in mountain environments (Teutschbein and Seibert, 2012; Chen et al., 2013; Shrestha et al., 2017). Temperature for a given time 't' ($T_{(t)}$) is corrected with an additive factor ($\overline{T}_m - \overline{T}_s$, Eq. 1, where $\overline{T}_m$ is the average monthly historical air temperature observed at the reference weather station, and $\overline{T}_s$ represents the average monthly historical air temperature simulated by the CanESM5 for the grid cell occupied by the observation station), whereas the precipitation variables ($P_{(t)}$), are corrected with a multiplicative factor ($\overline{P}_m/\overline{P}_s$, Eq. 2, where $\overline{P}_m$ is the historical monthly hydroclimatic data average measured at the reference weather station, and $\overline{P}_s$ represents the monthly average simulated by the CanESM5). The use of additive (to correct the bias on the air temperature) and multiplicative (to correct the bias on other hydroclimatic variables) factors has been used in studies of hydrological impacts due to climate change (Teutschbein and Seibert, 2012; Fiseha et al., 2014; Althoff et al., 2020). Thus, bias-correction through the LSM was performed for both the baseline (1984–2014) and scenario (2015–2040) periods using Eqs. 1 and 2 (* represents the bias-corrected variable):

$$T^*_{(t)} = T_{(t)} + \overline{T}_m - \overline{T}_s \quad (1)$$

$$P^*_{(t)} = P_{(t)} \left(\frac{\overline{P}_m}{\overline{P}_s} \right) \quad (2)$$

Moreover, the seasonal (Spring: April 01 to May 15; Summer: May 16

Table 2
Confusion matrix with commission and omission errors between the reference and projected land cover change of 2020's during summer (i.e., late-May to July).

Classes	OW-M	OW-WM	OW-WS	M-OW	M-WM	M-WS	WM-OW	WM-M	WM-WS	WS-OW	WS-M	WS-WM	Marginal total	Comission error	Total accuracy	Kappa index
OW-M	83	2	1	1	2	1	2	1	2	2	1	2	100	0.17	85.1 %	0.84
OW-WM	3	84	1	1	2	1	1	1	2	1	1	2	100	0.16		
OW-WS	2	0	81	2	4	3	3	1	1	0	2	1	100	0.19		
M-OW	1	1	1	86	1	0	0	2	2	2	3	1	100	0.14		
M-WM	1	3	2	3	84	3	1	2	1	0	0	0	100	0.16		
M-WS	0	2	0	1	1	89	2	2	1	0	0	2	100	0.11		
WM-OW	0	2	1	1	3	0	84	1	2	2	2	2	100	0.16		
WM-M	1	1	0	1	1	1	2	86	2	2	1	2	100	0.14		
WM-WS	1	1	1	1	2	1	1	2	85	2	1	2	100	0.15		
WS-OW	0	0	2	1	1	2	0	2	2	84	3	3	100	0.16		
WS-M	0	1	2	1	1	2	1	3	1	2	86	0	100	0.14		
WS-WM	2	1	2	1	1	1	1	2	2	2	1	84	100	0.15		
Marginal total	94	98	94	100	103	104	98	105	103	99	101	101	1200			
Omission error	0.12	0.14	0.14	0.14	0.18	0.14	0.14	0.18	0.18	0.15	0.15	0.17				

to July 31; Late Summer: August 01 to September 15) historical LC (maps were obtained from Rodrigues et al. (2024)), from 1984 to 2022, which were used in the Artificial Neural Network (ANN) algorithm to project seasonal spatial LC. The four LC classes are: open water; marsh (*Schoenoplectus tabernaemontani* — bulrush, and *Typha latifolia* — Cattail Marsh); wet meadow (*Carex rostrata* — Beaked Sedge, *Carex aquatilis* — water sedge, *Equisetum arvense* — horsetail); woody/shrub vegetation (woody species: cottonwood — *Populus*, Norway spruce — *Picea abies*, and dogwood — *Cornus* spp.; shrub species: Sitka Willow — *Salix sitchensis*, Red — Osier dogwood — *Cornus sericea*, horsetail — *Equisetum* spp.). In addition, the ANN model incorporated terrain driving factors such as elevation (from the NASA SRTM Digital Elevation Model — DEM), slope, topographic position index (TPI — the difference between the elevation of each pixel and the average elevation of its neighbouring pixels (De Reu et al., 2012)), and aspect (suggested by Kamaraj and Rangarajan, 2022). The driving factors were created from the DEM using the Spatial Analyst tool in ArcGIS Pro v3.3.1. The ANN learns and applies spatial relationships between LC types, driving factors, and LC change across the study area, thus improving predictions (Gharaibeh et al., 2020).

The following is a succinct explanation of the terrain driving factors that were used in the ANN routine: elevation affects vegetation and land cover, with locally high elevations (e.g., on the riverbank) tending to display distinct vegetation types (e.g., woody and shrub) compared to nearby or adjacent low elevations (e.g., marsh). Slope affects floodplain land cover since taller dense vegetation is more prevalent on sloped terrain, for example, whereas open water is found in flat areas. Aspect can provide an index of local growing conditions due to solar radiation receipt, for example. TPI can provide a local proxy of hillslope-scale moisture conditions in flatter terrain, with local lowlands tending to be wetter and local uplands tending to be drier.

2.3. Modelling framework

The research was conducted in four stages (Fig. 2). First, an artificial neural network (ANN) approach, MOLUSCE (NextGIS, 2017) was used to project the spatial land cover (LC) using historical LC classification data from the UCRW (Rodrigues et al., 2024). Second, linear LC (i.e., Open Water, Marsh, Wet Meadow, and Woody/Shrub) simulation was performed using ANN. Third, hydroclimate-based models were created to project river discharge using T_{air} and P from the RCP 4.5 and 8.5 scenarios. Finally, trend analyses were performed to assess the impact of climate change based on the linear LC change and RCP scenarios.

2.4. Stage 1: linear LC projection using MOLUSCE

The MOLUSCE plug-in, integrated into the QGIS software (version 2.18), was employed to forecast changes in land cover (LC) of the UCRW until the 2040s. Historical seasonal LC maps (Rodrigues et al., 2024) were used along with terrain driving factors (Fig. S1A) to predict land-cover change. This projection utilises a hybrid approach combining artificial neural networks (ANN) and cellular automata (CA). The cellular automata (CA) functionality in QGIS is implemented using the Markov chain technique, which predicts future land cover based on past and current land cover (Yatoo et al., 2020). This model integrates seasonal historical and current land cover maps with spatial terrain driving factors (i.e., elevation, slope, topographic position index, and aspect; Supplementary material A) to provide estimates of future changes as tables and maps (Gašparović and Jogun, 2017). Moreover, the ANN algorithm in MOLUSCE was used since it tends to be more accurate than other techniques for LC prediction (Gharaibeh et al., 2020; Ahmad et al., 2023).

The parametrization of MOLUSCE begins with the transition potential model (i.e., the potential of a pixel to change from one land cover class to another), which was trained using a momentum of 0.05 (varying from 0 to 1), a learning rate of 0.01 (range between 0 and 1) to stabilise the learning graph (as per Alshari and Gawali, 2022; Kamaraj and Rangarajan, 2022) and was trained for 100 iterations to prevent overfitting. The learning rate, momentum, and iterations are called the learning parameters. High learning rate and momentum enable quick yet unstable learning; Small learning rate and momentum suggest steady yet sluggish learning. The number of iterations should avoid overfitting, which may be determined via testing and simulations. (NextGIS, 2017). A neighbourhood value (counts the pixels around the current pixel: size = 1 indicates 9 pixels, or 3 × 3 region; size = 2 implies 25 pixels, or 5 × 5 region, etc.) of 3 (i.e., which implies 49 pixels, or 7 × 7 region, from the historical LC dataset) was employed to train the ANN algorithm using change observations occurring within a 90-m radius around each LC cell. The model had 12 hidden layers (as per Muhammad et al., 2022), which were neurons that learned linear and non-linear relationships between the input (LC and terrain driving factors) and the output (projected LC). Each hidden layer neuron gets inputs from all previous layer neurons, multiplies them by their weights, adds a bias term, and sends the output via an activation function. Neuron output feeds the next layer (NextGIS, 2017). The projected LC pixel was decided based on the present state of a neighbouring cell, the changes in the surrounding cells, and by the relationships with the terrain driving factors in the CA framework (Lau and Kam, 2005; Koomen and Beurden, 2011).

The ANN-CA simulation was subsequently followed by the validation process, which allows for the verification, comparison, and validation of

Table 3
Confusion matrix with commission and omission errors between the reference and projected land cover change of 2020's during late summer (i.e., August to late-September).

Classes	OW-M	OW-WM	OW-WS	M-OW	M-WM	M-WS	WM-OW	WM-M	WM-WS	WS-OW	WS-M	WS-WM	Marginal total	Comission error	Total accuracy	Kappa index
OW-M	86	1	1	1	1	1	2	1	1	2	1	2	100	0.14	86.8 %	0.86
OW-WM	3	84	1	1	2	1	1	1	2	1	1	2	100	0.16		
OW-WS	2	0	85	1	1	3	3	1	1	0	2	1	100	0.15		
M-OW	1	1	1	86	1	0	0	2	2	2	3	1	100	0.14		
M-WM	1	3	1	2	89	1	1	1	1	0	0	0	100	0.11		
M-WS	0	2	0	1	1	89	2	2	1	0	0	2	100	0.11		
WM-OW	0	2	1	1	1	0	86	1	2	2	2	2	100	0.14		
WM-M	1	1	0	1	1	1	2	86	2	2	1	2	100	0.14		
WM-WS	1	1	1	1	2	1	1	2	85	2	1	2	100	0.15		
WS-OW	0	0	2	1	1	2	0	1	2	89	1	1	100	0.11		
WS-M	0	1	2	1	1	2	1	3	1	2	86	0	100	0.14		
WS-WM	0	1	1	0	1	2	1	1	1	1	1	90	100	0.10		
Marginal total	95	97	96	97	102	103	100	102	101	103	99	105	1200			
Omission error	0.09	0.13	0.11	0.11	0.13	0.14	0.14	0.16	0.16	0.14	0.13	0.14				

the projected LC. The validation process involved comparing the projected seasonal LC with the reference seasonal LC maps (Rodrigues et al., 2024). To avoid noise in the trends, approximate 20-year periods (1980s to 2020s) were used to forecast seasonal LC maps during the period from 2020 to 2040. The mode of the seasonal LC maps from the 1984 to 1988 (herein referred to as 1980s) and the 2002 to 2006 period (herein referred to as 2000s) was utilized to project the seasonal mode LC map from the 2018 to 2022 period (herein referred to as 2020s). This approach avoids the selection of a dry or wet year and instead uses 'typical' characteristics on a per pixel basis. Furthermore, the rationale for using these past intervals and years was based on an analysis of the Pacific Decadal Oscillation, which pinpointed normal, dry and wet years in the UCRW, as detailed by Rodrigues et al. (2024). For instance, in the 1980s, there were two normal years (1984 and 1988), two dry years (1985 and 1987), and one wet year (1986). In the 2000s, there was one normal year (2003), two dry years (2004 and 2005), and two wet years (2002 and 2006). In the end, ensuring a well-balanced combination of all floodplain conditions.

The mode of the LC maps was determined in the Google Earth Engine using the "*.mode()*" tool. Hence, the LC map for the year 2020 was derived utilising the reference LC mode and change maps from the 1980s and 2000s, and the terrain driving variables, as the input data using the prediction methodology described above. The predicted seasonal mode map of 2020's, was compared to the reference seasonal mode map of 2020's. The Kappa coefficient was employed to assess the level of accuracy between the reference and projected LC. Specifically, 100 pixels per land cover class were evenly random dispersed throughout the valley, resulting in a total of 400 pixels across the four land cover classes: open water, marsh, wet meadow, and woody/shrub. In addition, the Kappa coefficient was used to assess the accuracy between the projected land cover changes and the actual changes. This involved randomly selecting 100 points per class (1200 total), evenly random distributed across twelve LC change classes: 1) open water to marsh, 2) open water to wet meadow, 3) open water to woody/shrub, 4) marsh to open water, 5) marsh to wet meadow, 6) marsh to woody/shrub, 7) wet meadow to open water, 8) wet meadow to marsh, 9) wet meadow to woody/shrub, 10) woody/shrub to open water, 11) woody/shrub to marsh, and 12) woody/shrub to wet meadow. The analysis focused on the land cover areas that underwent change by excluding areas that retained the same LC class through time. The comparison was made between the reference land cover change map from the 2000s to the 2020s, and the land cover change map between the reference land cover from the 2000s and the projected land cover for the 2020s.

To extend the forecasts beyond 2020, the reference seasonal mode LC map from the 2000s and 2020s was used to forecast the seasonal mode LC map for the 2040s (i.e. 2038 to 2042). Fig. 3 illustrates the implementation of the cascade projection method.

2.5. Stage 2: hydroclimatic-based models for river discharge

Hydroclimatic models based on average monthly air temperature (T_{air}) (°C) and monthly total precipitation (P) (mm) were created to estimate monthly river discharge in the UCRW, since glacier melt, snow melt, and rainfall are the main drivers of river discharge (Diomede et al., 2008; Zhang et al., 2011; Tsuruta and Schnorbus, 2021). The seasonal (spring, summer, and late summer) models to simulate monthly river discharge were developed based on observed river discharge at Nicholson streamflow-gauge (from 1984 to 2022) as the response variable, T_{air} and P as inputs. T_{air} and river discharge were averaged, and cumulative P was totalised for each season (Spring; Summer; Late Summer). Average discharge (in $m^3 \cdot s^{-1}$) was projected for each season.

The seasonal models were created using the LABFit software (Silva et al., 2004), which uses the Levenberg-Marquardt optimisation technique (Levenberg, 1944; Marquardt, 1963) (also referred to as damped least-squares). This method is considered powerful because it combines a gradient descent algorithm, which is a machine learning approach

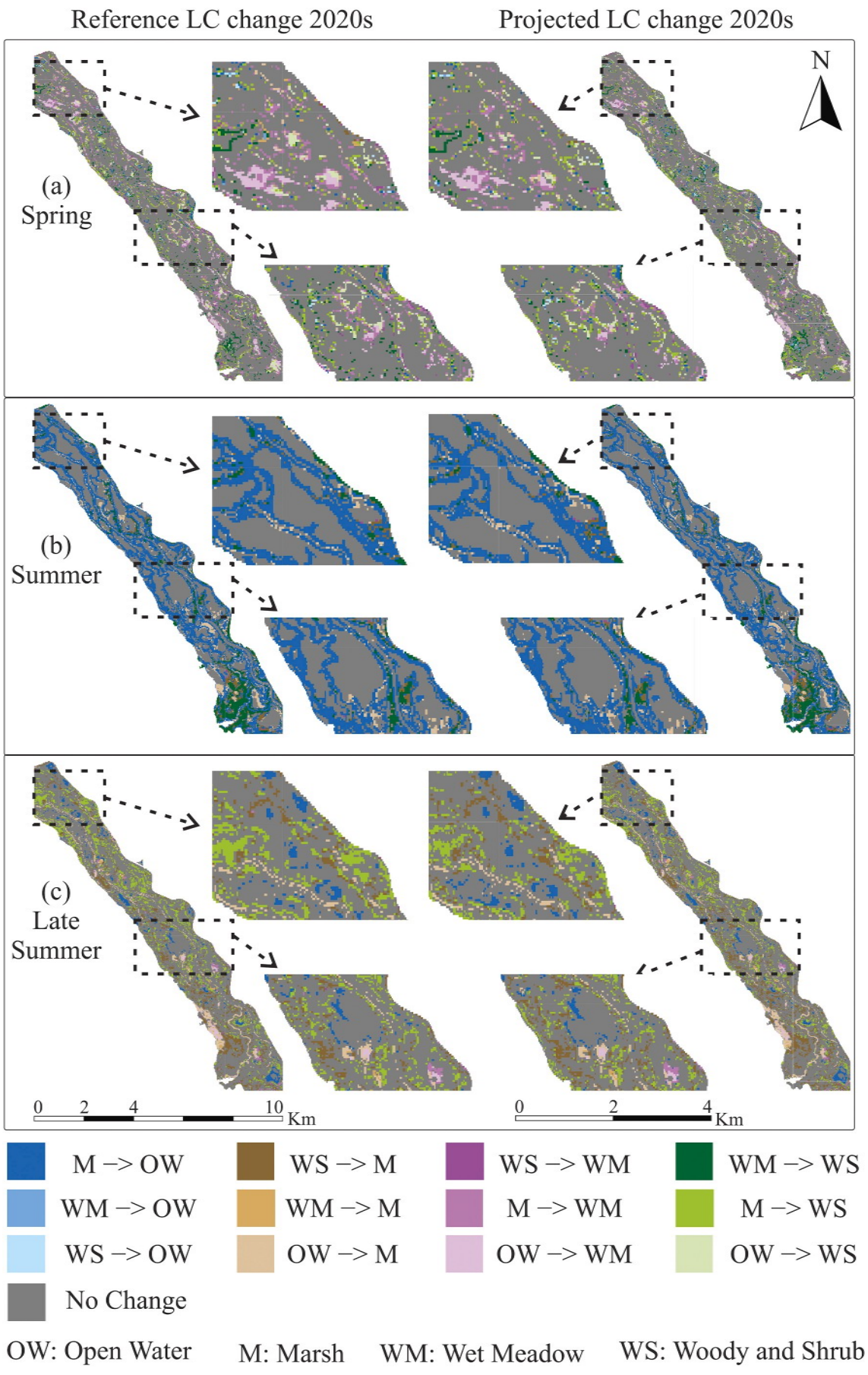

(caption on next page)

Fig. 5. Comparison of the reference and projected land cover change map of central section (portion of Spillimacheen to Golden, spanning a ~ 14 km stretch) of the UCRW from 2000's to 2020 during spring (a), summer (b), and late summer. M → OW: marsh to open water; WM → OW: wet meadow to open water; WS → OW: woody/shrub to open water; WS → M: woody/shrub to marsh; WM → M: wet meadow to marsh; OW → M: open water to marsh; WS → WM: woody/shrub to wet meadow; M → WM: marsh to wet meadow; OW → WM: open water to wet meadow; OW → WS: open water to woody/shrub; M → WS: marsh to woody/shrub; and WM → WS: wet meadow to woody/shrub.

Table 4
Comparison of the reference and projected LC change extent maps from the 2000s to 2020s in the Upper Columbia River floodplain.

LC change classes	Reference LC change (km^2) (Rodrigues et al., 2024)			Projected LC change (km^2)			TE (km^2)			%TE (%)		
	S	Su	LS	S	Su	LS	S	Su	LS	S	Su	LS
OW (no change)	22.10	46.00	24.70	22.00	46.20	24.30	−0.10	0.20	−0.40	−0.45	0.4	−1.6
OW → M	0.40	4.30	7.80	0.45	4.45	8.00	0.05	0.15	0.20	12.50	3.5	2.6
OW → WM	2.00	0.90	1.40	2.20	0.95	1.30	0.20	0.05	−0.10	10.00	5.6	−7.1
OW → WS	3.10	0.80	0.10	2.95	0.68	0.11	−0.15	−0.12	0.01	−4.84	−15.0	10.0
M (no change)	11.30	73.00	102.00	11.50	73.40	101.20	0.20	0.40	−0.80	1.77	0.5	−0.8
M → OW	5.90	5.80	1.40	5.50	6.20	1.30	−0.40	0.40	−0.10	−6.78	6.9	−7.1
M → WM	3.40	5.90	1.10	3.30	5.80	1.20	−0.10	−0.10	0.10	−2.94	−1.7	9.1
M → WS	4.00	13.30	8.50	3.80	13.10	9.30	−0.20	−0.20	0.80	−5.00	−1.5	9.4
WM (no change)	87.00	18.00	0.60	88.00	17.80	0.57	1.00	−0.20	−0.03	1.15	−1.1	−5.0
WM → OW	9.10	0.90	0.50	9.00	0.85	0.47	−0.10	−0.05	−0.03	−1.10	−5.6	−6.0
WM → M	6.90	0.70	0.20	6.60	0.65	0.21	−0.30	−0.05	0.01	−4.35	−7.1	5.0
WM → WS	8.00	1.40	2.30	7.80	1.50	2.32	−0.20	0.10	0.02	−2.50	7.1	0.9
WS (no change)	14.40	13.00	36.70	14.60	13.20	36.30	0.20	0.20	−0.40	1.39	1.5	−1.1
WS → OW	2.80	2.10	0.10	2.68	2.00	0.10	−0.12	−0.10	−0.01	−4.29	−4.8	−5.0
WS → M	2.20	1.90	0.10	2.28	2.00	0.09	0.08	0.10	−0.01	3.64	5.3	−10.0
WS → WM	5.10	0.20	0.10	5.20	0.21	0.11	0.10	0.01	0.00	1.96	5.0	5.0

S — spring; Su — summer; LS — late summer; OW: open water; M: marsh; WM: wet meadow; WS: woody/shrub.

used to find the coefficients of a function that minimises a cost function, with a Gauss-Newton algorithm, which solves non-linear least squares problems found by the minimum residual of the chosen non-linear function (Silva et al., 2004). The optimal non-linear regression form between the T_{air} and P and river discharge was determined based on the reduced chi-square (i.e., a non-linear function around 1 is ideal) using the LABFit library, which offers over 500 pre-defined non-linear regression functions. The river discharge data from 1984 to 2022 were divided into two equal parts: 50 % for training (even years 1984, 1986, etc.) and the remaining 50 % (odd years) for validation. Training and validation were sampled from alternating years to mitigate the influence of anomalous multi-year periods, and due to a noticeable shift in the UCRW river flow patterns around the year 2000 (Rodrigues et al., 2024).

2.6. Stage 3: river discharge and open water extent forced with RCPs 4.5 and 8.5

The seasonal hydroclimatic-based models from Section 2.4, were driven by the bias corrected T_{air} and P from CanESM5 (from historical, 1984–2014, and projected 2015–2040). The river discharge was examined using two distinct atmospheric forcing scenarios: a hydroclimatic-based model driven by the RCPs 4.5 (SSP2) and 8.5 (SSP5). To determine if projected river flow was representative of true discharge, GCM-modelled discharge at RCP 4.5 and 8.5 was compared (using Nash-Sutcliffe coefficient) against observed discharge during the period of overlap from 1984 to 2022.

Total floodplain open water extent for each season was estimated for both RCP 4.5 and 8.5 scenarios using previously generated empirical models (Rodrigues et al., 2024) of open water area based on river discharge (i.e., river discharge vs open water regression; herein referred to as regression model). GCM-modelled open water extent was compared to the open water extent projected by the ANN approach, which determined the RCP pathway that the linear projection of the UCRW followed in the future.

2.7. Stage 4: trend analyses

The Mann-Kendall method (Kendall, 1957; Mann, 1945) was used to conduct a trend analysis on the projected LC extent, GCM-modelled river discharge, open water area, air temperature and precipitation in pyMannKendall (Hussain and Mahmud, 2019). The Mann-Kendall method evaluates three hypotheses: i) the absence of a trend (null hypothesis), ii) a positive trend, and iii) a negative trend. A significance threshold of p-value = 0.05 was adopted. The magnitude of the changes was evaluated by the nonparametric Sen's slope and Kendall's tau (τ) coefficient, which quantifies the association between the variables.

2.8. Statistical comparisons

In Section 2.4, the reference and projected LC extent (in square kilometres) for the 2020's were compared using two statistical techniques: Total error (TE) and Total Percentage Error (%TE).

In Section 2.5, the hydroclimatic model performances were assessed using the coefficient of determination (R^2), RMSE, the Nash-Sutcliffe coefficient (NSE) as proposed by Nash and Sutcliffe (1970), and the percent RMSE (%RMSE).

In Section 2.6, the open water extent projected by RCP 4.5 and 8.5 was compared to the open water extent projected by the ANN approach utilising the RMSE and %RMSE. This comparison determined the RCP pathway that the linear projection of the UCRW followed in the future.

3. Results

3.1. Spatial LC projection accuracy

The seasonal kappa coefficients of the predicted raster for the 2020's (using the LC of 1980's and 2000's from each season) over the spring, summer and late summer seasons was 0.86, 0.88, and 0.81, respectively. The seasonal confusion matrix with total accuracy, omission and commission errors of the reference and projected land cover of 2020s are shown in Supplementary material B. Moreover, Fig. 4 illustrates the seasonal (spring, summer, and late summer) predicted LC for each floodplain land cover compared to the reference dataset.

More importantly, the seasonal kappa coefficients of the LC change maps (i.e., between the reference and projected 2000's and 2020's) during spring, summer, and late summer was 0.78, 0.84, and 0.86,

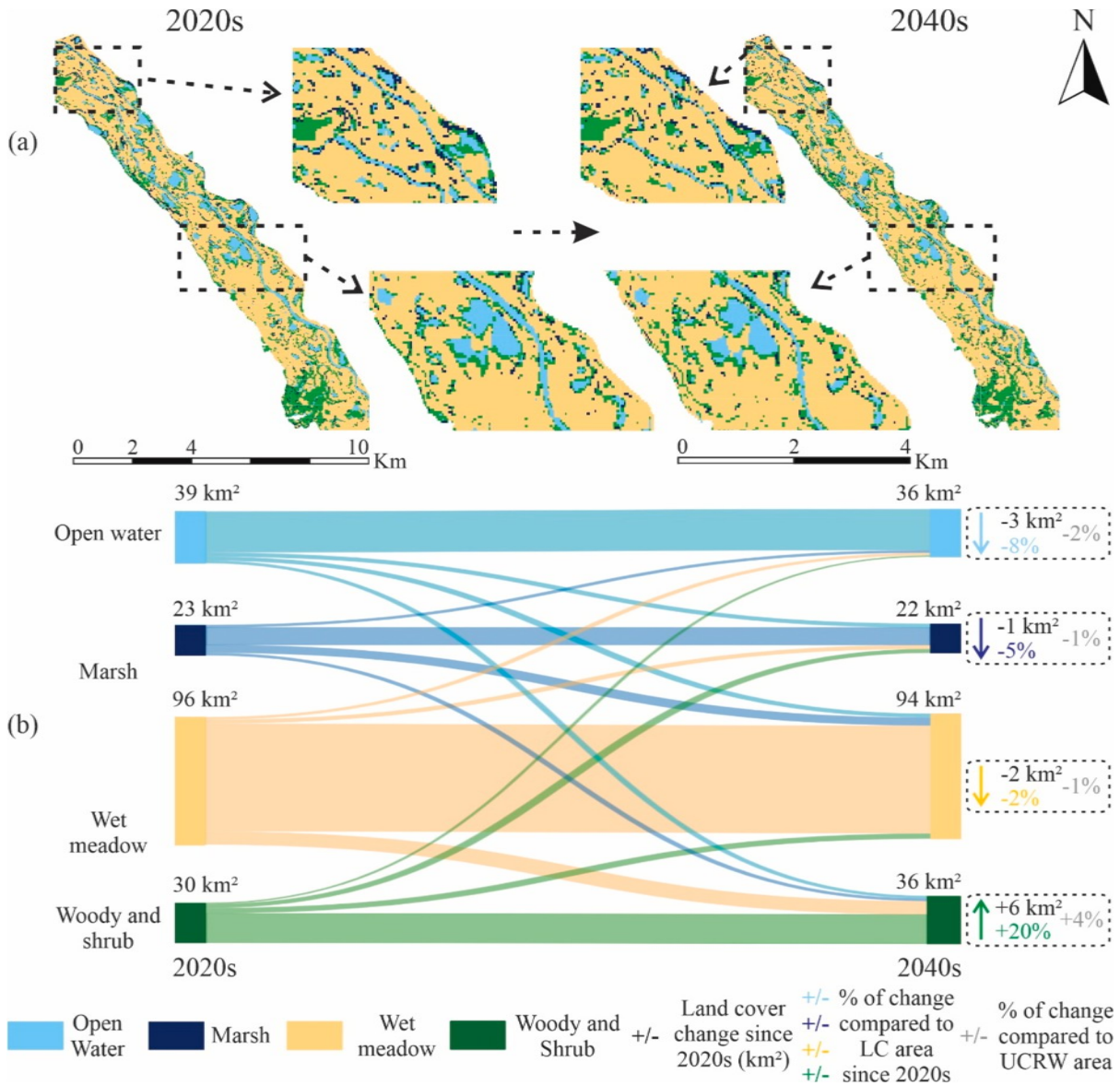

Fig. 6. Projected UCRW land cover change from April to mid-May. Insets: a) illustrate changes in land cover for a central sample region (~14 km stretch portion of Spillimacheen to Golden) of the overall floodplain. b) Sankey diagram depicting the land cover change from 2020 to 2040, the land cover change since 2020, and the percentage of change compared to each individual land cover since 2020, and the UCRW area (188 km^2).

respectively. Tables 1 to 3 describe the seasonal (spring, summer, and late summer) confusion matrix with total accuracy, omission and commission errors of the reference and projected land cover change maps from 2000s to 2020s. In addition, Fig. 5 illustrates the seasonal (spring, summer, and late summer) predicted LC change map for each floodplain land cover compared to the reference LC change map dataset.

Table 4 shows that the projected LC of 2020's total errors (TE) between −0.8 and +1.0 km^2 (average: +0.03 km^2), with total percentage errors (%TE) varying from −15 % to +12.5 % (average: −0.1 %). The best projected land cover change classes were as follows: Spring: wet meadow to open water; Summer: marsh to woody/shrub; Late summer: open water to marsh. Also, in Spring, open water to marsh and wet meadow change trajectories were overestimated, while during summer there was an under-estimation of the open water to woody/shrub change class. In late summer an overestimation of marsh to wet meadow and marsh to woody/shrub was found. These results match commission and omission outcomes, i.e., Tables 1 to 3. Therefore, the projected LC extents are a reasonable representation of the reference (or true) LC.

3.2. *Projected floodplain landcover change from 2020 to 2040*

From 2020 to 2040, the area of open water is predicted to decrease in spring (April to mid-May) (−3 km^2 or −2 % of the total floodplain area) and late summer (August to mid-September), while an increase is expected during summer season (late-May to July) (−9 km^2 or −5 %). Marsh areas are projected to decrease during the spring (−1 km^2 or −1 %), summer (−19 km^2 or −12 %), and late summer (−2 km^2 or −1 %). Wet meadow area is projected to decrease during spring (−2 km^2 or −1 %) and increase in the summer (+6 km^2 or +4 %), and late summer (+1 km^2 or −1 %). On the other hand, the area of woody/shrub vegetation increased during the spring (+6 km^2 or +4 %), summer (+7 km^2 or +4 %), and late summer (+10 km^2 or +5 %). The air temperature and precipitation are projected to increase. The changes per season of the land cover extent are depicted in Figs. 6, 7, and 8, and the trends in the hydro-climatological parameters are shown in Table S4 (Supplementary Material C).

A section-based evaluation (i.e., Invermere to Brisco, Brisco to Spillimacheen, Spillimacheen to Golden, Golden to Donald) of the

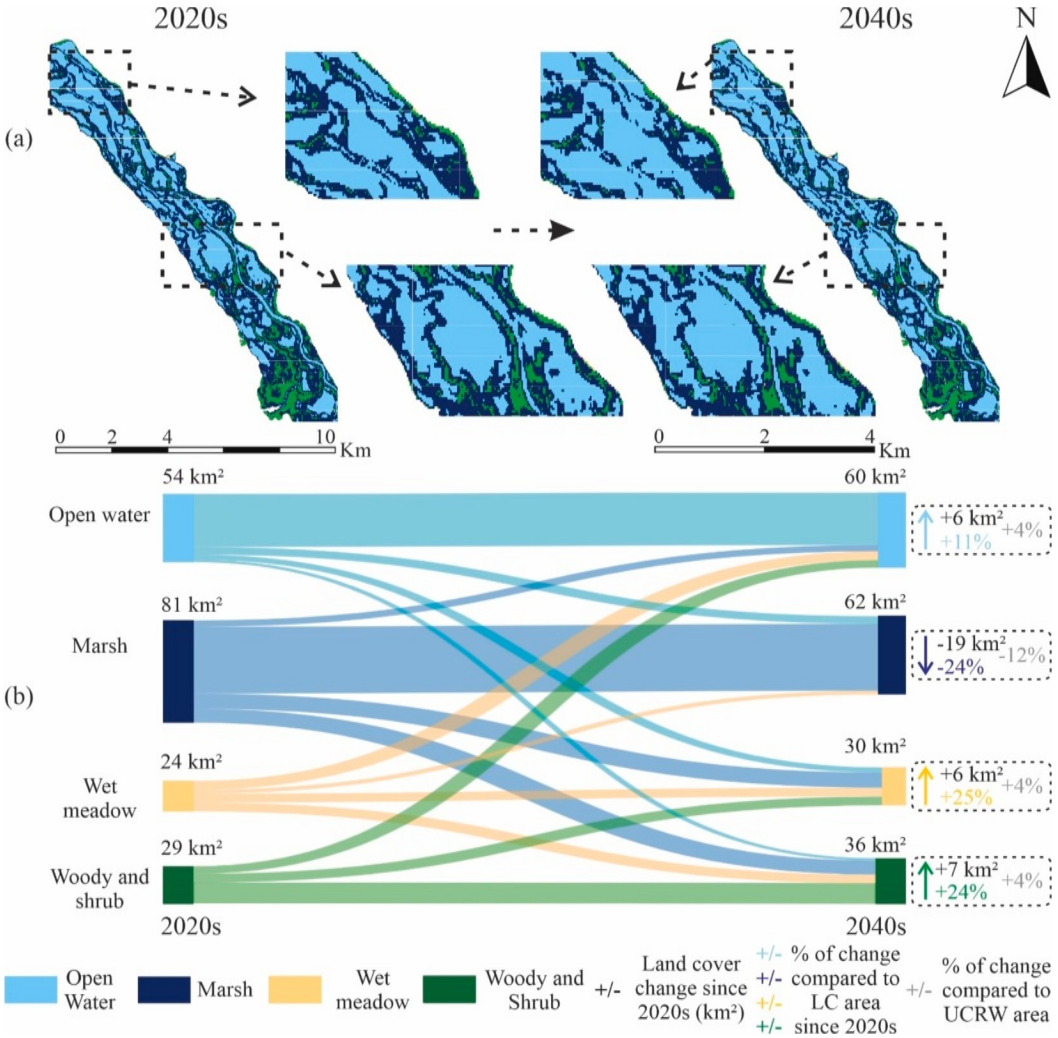

Fig. 7. Projected UCRW land cover change from late-May to July. Insets: a) illustrate changes in land cover for a central sample region (~14 km stretch portion of Spillimacheen to Golden) of the overall floodplain. b) Sankey diagram depicting the land cover change from 2020 to 2040, the land cover change since 2020, and the percentage of change compared to each individual land cover since 2020, and the UCRW area (188 km^2).

UCRW was conducted, showing the projected changes per river reach section of the floodplain from 2020 to 2040. Based on this, the most vulnerable section of the UCRW is from Spillimacheen to Golden (supplementary material D in Fig. S2), which during spring is projected to have larger decreases in open water, marsh, and wet meadow, and increases in woody/shrub. During the summer, open water, wet meadow, and woody/shrub are likely to increase, while marsh areas will decrease. Meanwhile, in late summer, open water and marsh are expected to decline, while wet meadow and woody/shrub encroachment will increase. In addition, the second most vulnerable section is from Brisco to Spillimacheen, followed by Invermere to Brisco, and Golden to Donald. The other projected land cover changes per section and season results are described in supplementary material D, Figs. S3 (Invermere to Brisco), S4 (Brisco to Spillimacheen) and S5 (Golden to Donald).

3.3. River discharge model

Fig. 9(a, b, c) presents the training and validation performance of the seasonal Upper Columbia river discharge models trained from monthly air temperature and precipitation. The model for spring had the highest accuracy, followed by late summer, then summer. Fig. 10d shows a visual comparison between modelled versus reference values of river discharge at the Upper Columbia River. The higher precision of the hydroclimatic models during spring is due to low flow variation during this season, which makes it simpler to simulate. While in late summer and summer, river flow is more dynamic. Overall, the results suggest that the seasonal hydroclimatic-based models captured the river dynamic throughout the 1984 to 2022 period.

3.4. Projected discharge trends forced by RCP 4.5 and 8.5

The projected Upper Columbia River discharge changes from 1984 to 2040 are illustrated in Fig. 10 during the spring (Fig. 10a), summer (Fig. 10b), late summer (Fig. 10c). In the spring, the Upper Columbia River discharge tends to increase under RCP 4.5 (+0.78 m^3 s^{-1} year^{-1}) and 8.5 (+1.85 m^3 s^{-1} year^{-1}). However, the river discharge during summer (RCP 4.5: −1.13 m^3 s^{-1} year^{-1}; RCP 8.5: −1.32 m^3 s^{-1} year^{-1}) and late summer (RCP 4.5: −0.03 m^3 s^{-1} year^{-1}; RCP 8.5: −0.21 m^3 s^{-1} year^{-1}) season are projected to reduce. Overall, regardless of the scenarios and season, almost all river discharge projections out to 2040 (except for the RCP 4.5 in late summer) are statistically significant ($p < 0.05$).

Furthermore, when comparing the modelled and measured overlapping period of river discharge (i.e., from 1984 to 2022), during spring, the RCP 4.5 (NSE 0.73) better represented the reference river discharge, followed by the RCP 8.5 (R^2 0.65) projections. In summer, the RCP 4.5 paths better reflected the reference discharge, with NSE of 0.49, while RCP 8.5 projections had a lower precision, NSE of 0.40. Over the

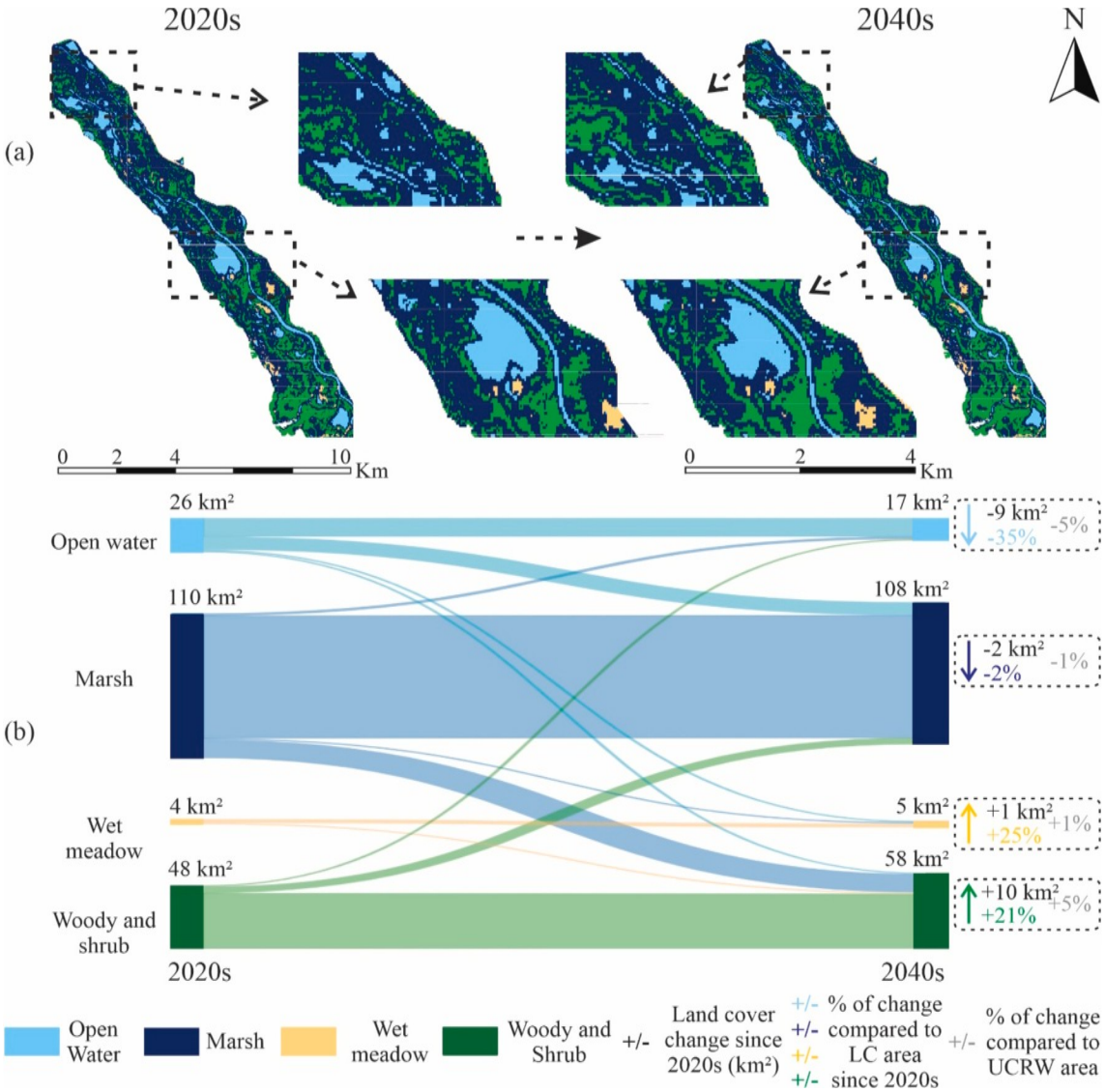

Fig. 8. Projected UCRW land cover change from August to mid-September. Insets: a) illustrate changes in land cover for a central sample region (~14 km stretch portion of Spillimacheen to Golden) of the overall floodplain. b) Sankey diagram depicting the land cover change from 2020 to 2040, the land cover change since 2020, and the percentage of change compared to each individual land cover since 2020, and the UCRW area (188 km^2).

late summer, the RCP 4.5 (NSE 0.63) were better associated with the reference river discharge, and a low representation by the RCP 8.5 (NSE 0.54).

3.5. Projected floodplain open water area trends forced by RCPs 4.5 and 8.5

The open water extent of the UCRW from 1984 to 2040 is shown in Fig. 11, during the spring (Fig. 11a), summer (Fig. 11b), late summer (Fig. 11c). In the spring, the open water area will increase according to the RCP 4.5 (+0.21 km^2 year^{-1}) and 8.5 (+0.30 km^2 year^{-1}). In contrast, the open water extent during summer (RCP 4.5: −0.05 km^2 year^{-1}; RCP 8.5: −0.06 km^2 year^{-1}) and late summer (RCP 4.5: −0.07 km^2 year^{-1}; RCP 8.5: −0.10 km^2 year^{-1}) season will decrease. Overall, all projected trends of open water extent are statistically significant ($p < 0.05$), independent of the scenarios and seasons with the exception of the late summer period.

Fig. 11 illustrates the comparison between the predicted open water extent determined by the Artificial Neural Networks (ANN) findings and the open water projected by both RCPs paths. Overall, the open water LC extent based on ANN were well within the 95 % confidence limits of the RCP 4.5 open water area during spring, summer, and late summer. The ANN seasonal open water LC projections deviated further from the RCP 8.5 open water trend line with spring showing the greatest negative deviation.

Moreover, comparing the modelled and measured overlapping period of open water (i.e., from 1984 to 2022), RCP 4.5 better represented the reference open water extent in all seasons (NSE: spring 0.60, summer 0.44, and late summer 0.59) (Fig. 11a, b, c). Meanwhile, the RCP 8.5 paths showed lower precision over the spring (NSE 0.53), summer (NSE 0.33) and late summer (NSE 0.39) (Fig. 11a, b, c).

4. Discussion

4.1. MOLUSCE as a tool for land cover projection

The overall average kappa coefficient for the predicted LC made by the ANN method was 0.85, which is considered a good accuracy for wetlands (Alam et al., 2021; Rahman et al., 2017), as this ecosystem tends to be very dynamic and difficult to predict. In the spring, open

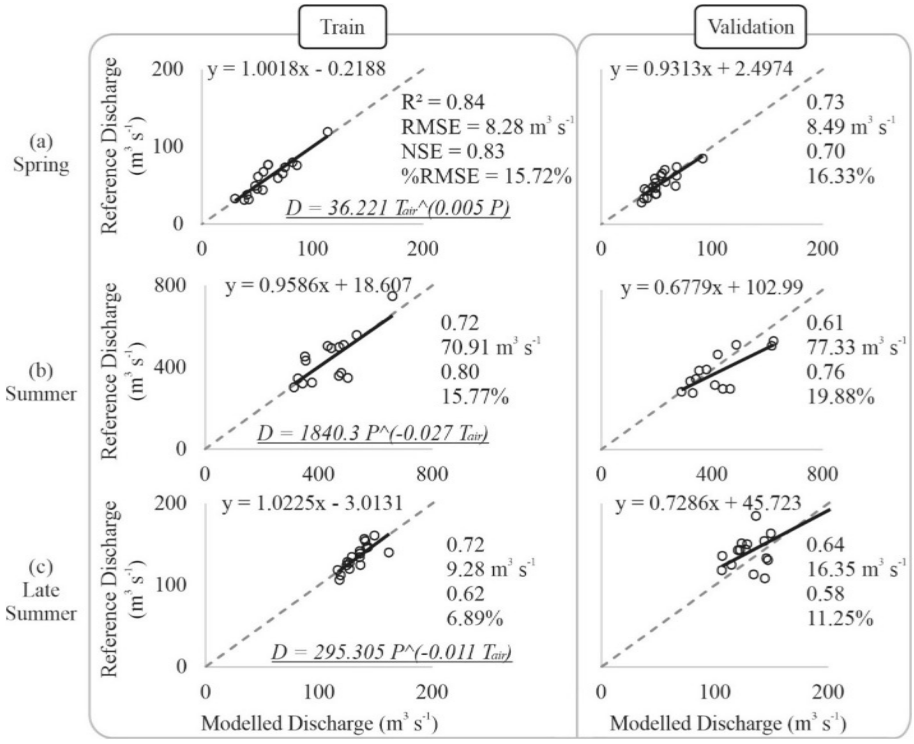

Fig. 9. Performance (i.e., R^2, RMSE, NSE, and %RMSE) of the seasonal hydroclimatic-based models for spring (a), summer/peak flow (b), and late summer (c), and the annual variation of reference and seasonal modelled (i.e., train and validation data) river discharge (d) from 1984 to 2022.

water, marsh, wet meadow, and woody/shrub were easier to discern. In summer, the wetlands are largely covered by open water, marsh, and woody/shrub vegetation, with a small area of wet meadow visible since high water levels cover the dominant wetland meadow vegetation. In late summer, marsh and woody/shrub vegetation greens up, confusing the vegetated groups. Furthermore, marsh and wet meadow merge, which may diminish late summer kappa values.

Regarding the 2000s–2020s seasonal LC change maps comparison, overall average kappa coefficient between the reference and predicted LC by the ANN method was 0.82. However, during the spring (0.78) and Summer (0.84) presented the lowest kappa. This may be explained as LCs changes throughout Spring and summer are more complex (i.e., with earlier shift of the peak discharge from summer to spring) than in Late Summer (kappa coefficient was the greatest, 0.86), when drying patterns are more predictable (as open water and marsh decrease, wet meadow and woody/shrub grow).

In addition, the projected open water areas in 2040 by the ANN approach and the regression model (i.e., river discharge vs open water) are better aligned with the RCP 4.5 predictions, exhibiting a historical (1984 to 2022) average NSE of 0.54. The results highlight the precision of the ANN in projecting the LC extent in the UCRW. Solely relying on the ANN technique would suggest that the wetlands will have reduced open water areas in spring and late summer, while experiencing increased open water throughout summer. However, as the ANN predictions are for a specific time interval (i.e., 2020s and 2040s), the real trend can be masked as wetlands are a fluctuating ecosystem, experiencing both dry and wet periods depending on the season and year. This variability is illustrated in Fig. 10, which displays the fluctuations in open water areas across the projected seasons and timeframe.

4.2. Climate change impacts on the Upper Columbia River floodplain

The projected increase of river discharge and open water during spring in the Upper Columbia River Wetlands (UCRW) are influenced by regional air temperature and precipitation, which since 2015 tend to increase by 0.5 °C and 3 mm, respectively, in the 2040s under RCP 4.5 and 0.8 °C and 5 mm in the 2040s under RCP 8.5. This pattern in the spring season may influence the timing of snowmelt in the UCRW, which usually starts in April (spring) and achieves a peak in June–July (summer), and then decreases through August and September (late summer).

The onset of snowmelt may shift to earlier in April as has been observed by Rodrigues et al. (2024) in the same region, who suggested that the peak flow occurred six days earlier in 2022 than in 1984, in addition, the peak flow duration has shortened by ~one day, with a higher frequency of high discharge events showing more rapid onset. In the UCRW, an earlier shift of the peak discharge from summer to spring is expected in under the RCP 4.5 and RCP 8.5 scenarios. In fact, in 2023, peak discharge in the Nicholson gauge occurred from May 9th to May 25th (as per Environment Canada, 2022c). Tsuruta and Schnorbus (2021) employed a sophisticated hydrological model that incorporated factors such as snow and glacier melt, as well as rainfall, to forecast river discharge in the Mica Basin, north of the UCRW, until the year 2100. The authors found that spring discharge will likely increase under both RCP 4.5 and 8.5 scenarios while summer and late summer discharge are projected to decrease in both scenarios, which aligns with our findings. In Keremeos Creek watershed, southern British Columbia (Canada), Mirmasoudi et al. (2019) observed an earlier timing of snowmelt regarding RCP 4.5 and 8.5 which is to be expected as a function of increasing air temperature. Thus, for RCP 4.5 in the 2040s, snowmelt may start earlier in March and peak in May. However, RCP 8.5 in the 2040s may cause snowmelt to begin sooner (February~May) and peak in April. In the Columbia watershed (above Donald), Bürger et al. (2011) projected an earlier snowpack melting, resulting in June peak discharges instead of July. The projected warming in this watershed is changing its hydrology from snow-melt-dominated (nival) river discharge to rainfall-driven (pluvial) discharge. In consequence, river discharge in August and September is projected to decrease. In the Spillimacheen, Schnorbus et al. (2012) projected in both scenarios an earlier spring freshet (April and May) and a peak discharge shift from July to June. As a result, July, August, and September 2050s river discharge is expected to decrease

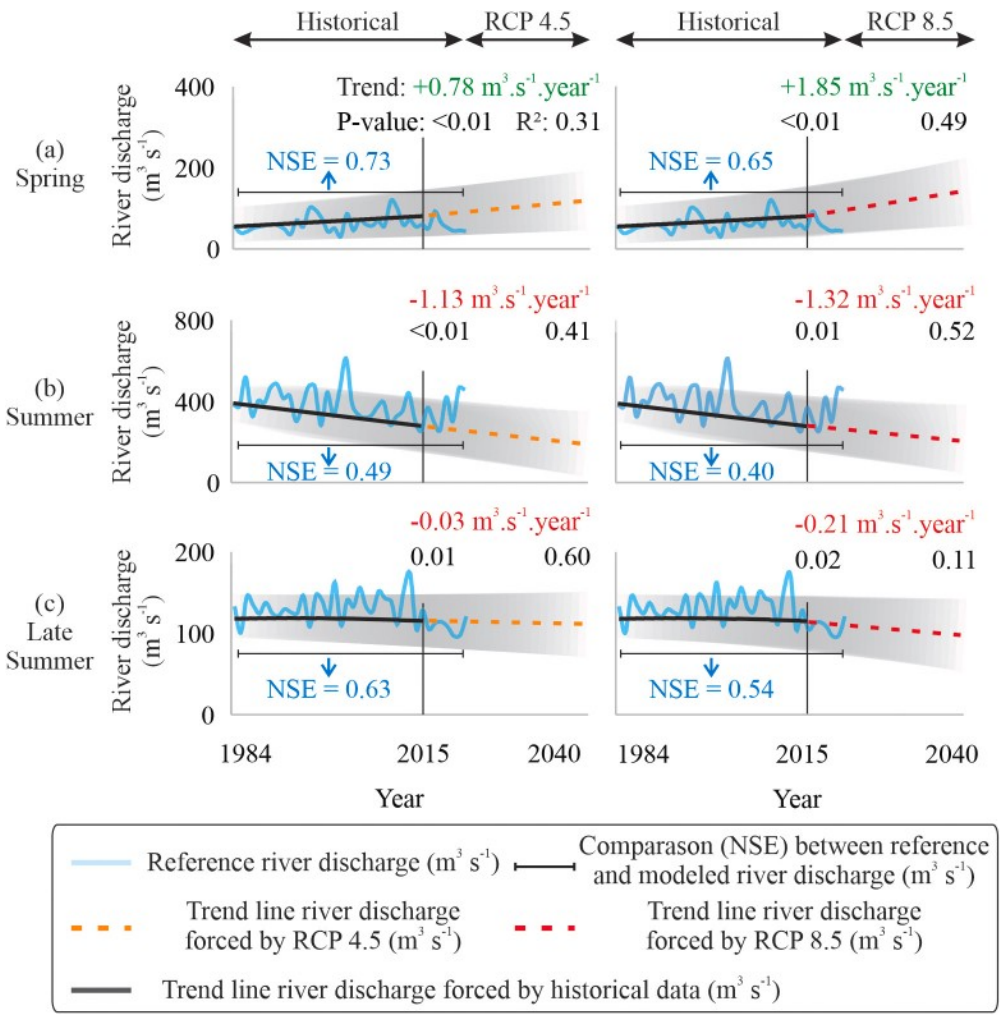

Fig. 10. Projected trends (1984–2040) of river discharge during spring (a), summer/peak flow (b), late summer (c) and forced by the RCPs 4.5 and 8.5, and a comparison (NSE) between reference and modelled river discharge (1984–2022). Shaded areas indicate the 95 % confidence intervals for the projected river discharge for each decade.

substantially.

The river reach section from Spillimacheen to Golden has changed the most, which is likely due to the discharge of the Spillimacheen river and Bugaboo snow and glacier melt streams, where there are a large number of downstream connected wetlands that can quickly respond to river discharge fluctuations. In the Columbia River Basin, glacier runoff generates 25–35 % of surface flows during late summer river discharge (Jost et al., 2012), supplying downstream wetlands (Fleming and Dahlke, 2014; Milner et al., 2017). However, from 1985 to 2005, Columbia Basin glaciers lost 15 % of their area (Bolch et al., 2010) and have been projected to decline 35 % to 100 % by 2100 (Clarke et al., 2015). These historical and forecast declines in glacier volume and area decreases threaten Columbia River tributaries and wetlands.

Worldwide, climate change will also impact river floodplain ecosystems, for instance, Moradkhani et al. (2010) employed the Soil and Water Assessment Tool in the Tualatin River floodplain (USA) to forecast river flow for a 50-year recurrence interval. The findings indicated a significant decrease (~−200 $m^3\ s^{-1}$) for low and middle emissions scenarios, while a notable increase (~+200 $m^3\ s^{-1}$) under high emissions scenario. In rainfall-driven river floodplains, multi-model projections (50–100 years) indicate that by mid-century, mean annual precipitation and runoff are expected to decrease by 10–30 % in certain dry subtropical and tropical regions, such as West Africa, Central America, and northeast Brazil, while an increase of 10–40 % is projected in some wet tropical regions, including equatorial Africa, the La Plata River, southern Asia, and northern Australia (Milly et al., 2005; Nohara et al., 2006; Li et al., 2007; Bates et al., 2008; Weiland et al., 2012). In the context of extensive river systems and using hydrological simulations, Booij (2004) in the Meuse River (which flows through France, Belgium, and the Netherlands) observed a small reduction in average discharge and a slight rise in discharge variability during extreme events. Meanwhile, Middelkoop et al. (2001) demonstrate that global warming will shift the Rhine River basin (Europe) from a combined rainfall and snowmelt regime to one that is predominantly dominated by rainfall. This shift is expected to result in higher winter discharge, more intense and earlier peak flows in spring, decreased summer discharge, and prolonged low flow during late summer.

The projected reduction of the river discharge is also a function of decreases in the ratio of snow to total monthly precipitation due to air temperature increases in all RCP projections (Flannigan et al., 2009; Schnorbus et al., 2012; Carver, 2017; Wang et al., 2017). If increased precipitation falls as rain, snow accumulation- and melt-dominated watersheds may be more controlled by rainwater runoff (Barnett et al., 2005; Stewart et al., 2005; Knowles et al., 2006; Hamlet et al., 2013; MacDonald et al., 2010), which may also increase the erosion in the mountains (Zhang et al., 2022a) enhancing siltation within the floodplain. Yet, recent studies observed the discharge response to positive trends of temperature, consequently, lower discharges were found during summer and late summer due to increased evaporation rates and a shift in the snow dynamics (Bach et al., 2018; Teuling et al., 2019),

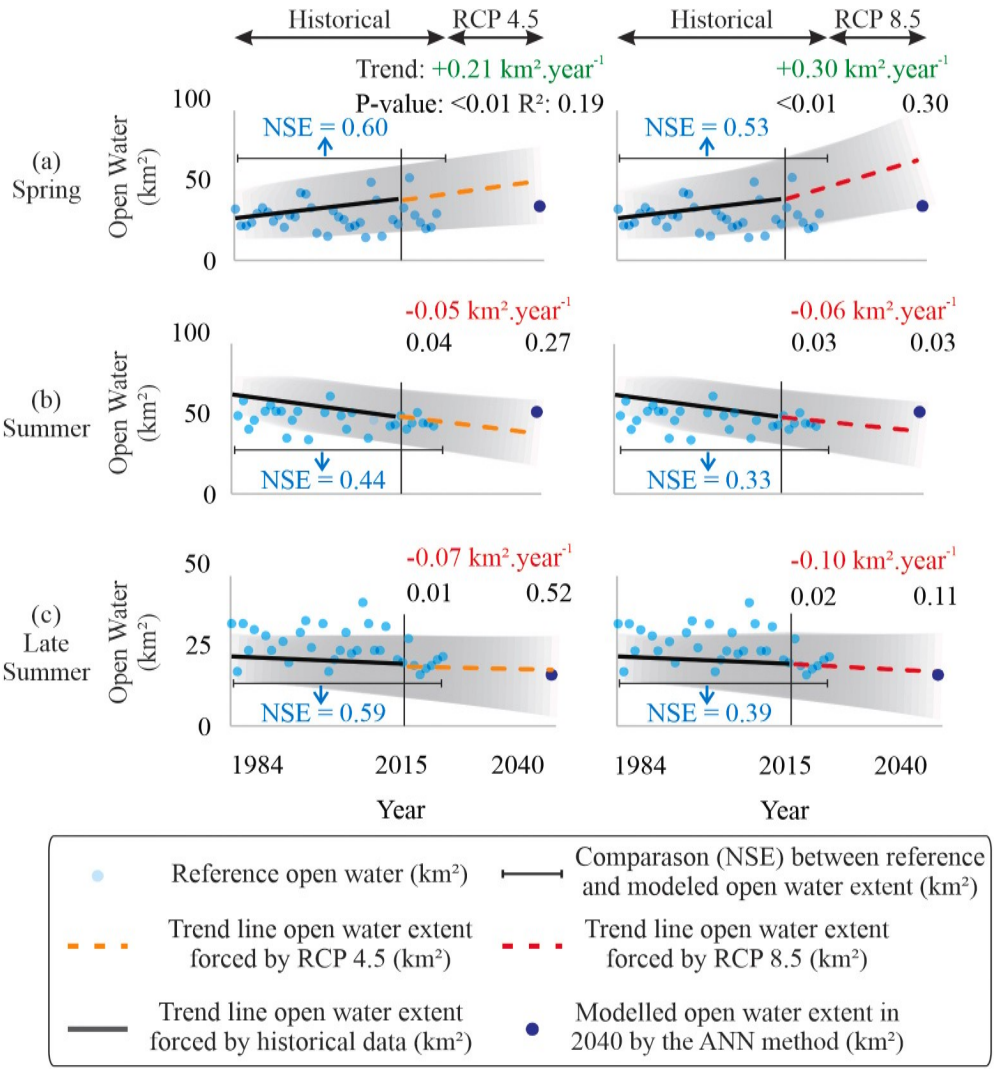

Fig. 11. Projected trends (1984–2040) of open water extent during spring (a), summer/peak flow (b), and late summer (c) forced by the RCPs 4.5 and 8.5, and a comparison (NSE) between reference and open water extent (1984–2022) and the ANN method in 2040. Shaded areas indicate the 95 % confidence intervals for the projected open water extent for each decade.

which may explain the decrease in permanent water bodies in the UCRW during late summer (Hopkinson et al., 2020).

The projected trends over the discharge and open water may directly affect marsh areas, which are located around these water bodies. Air temperature and precipitation are the main drivers for marsh extent, which may be explained as they react rapidly to hydrological and climatological changes (Keddy, 2011). The positive trends of rainfall and faster snowmelt in the UCRW may create larger open water areas but reduce the marsh fringe area essentially during spring and summer, as the floodplain will have a rapid overflow, submerging the whole marsh area (Keddy and Reznicek, 1986; Keddy, 2011; Van Der Valk, 2005) and a portion of small riparian woody and shrub vegetation (Sparks, 1995; Fischenich and Copeland, 2001; Steiger et al., 2005). Marsh zones may also be influenced by animals, for example beavers as they may control the open water pattern in some regions building dams, which can retain water regardless of the season (Hood and Bayley, 2008).

The close connection between floodplain open water and marsh areas suggests that if open water dries out, marshes will disappear, which has been observed by negative projected annual trend for both land covers. This negative trend in open water and marsh land covers will make room for wet meadow, which is forecasted to increase during summer and late summer and reduce in the spring (Clair et al., 1998; Kołos et al. 2013). Wet meadow area may increase during summer and late summer because the projected precipitation changes during spring (DeBeer et al., 2015, DeBeer et al., 2021), which will result in faster flooding in a shorter time period. In addition, increasing evaporation rates (Werner et al., 2013; Bach et al., 2018; Teuling et al., 2019) could reduce the area of open water, which may open some space for wet meadow in the end of summer and late summer when the open water levels will tend to be low.

Wet Meadow is an important ecosystem in the UCRW, providing many ecosystem services, for example, carbon sequestration (Wang et al., 2005), nutrient cycle (Zhang et al., 2022b), and aquifer recharge (McClymont et al., 2010). Nevertheless, due to drier conditions, woody/shrub encroachment in this region has been advancing since 1980s (Rodrigues et al., 2024), and according to the projections will continue, which may alter the community composition and structure of the floodplain's flora. The transition from herbaceous (i.e., marshes and wet meadows), to woody or shrub vegetation is not immediate (from one year to the next). Herbaceous plants can be perennials or annuals, and the ecological succession to a woody or shrub state may be dependent on previous conditions (wet or dry) of the floodplain and could exhibit delays, potentially spanning years (Rood et al., 2003). For instance, seeds of the cottonwood species are typically dispersed following the annual peak in river flows, when the receding flood exposes moist areas

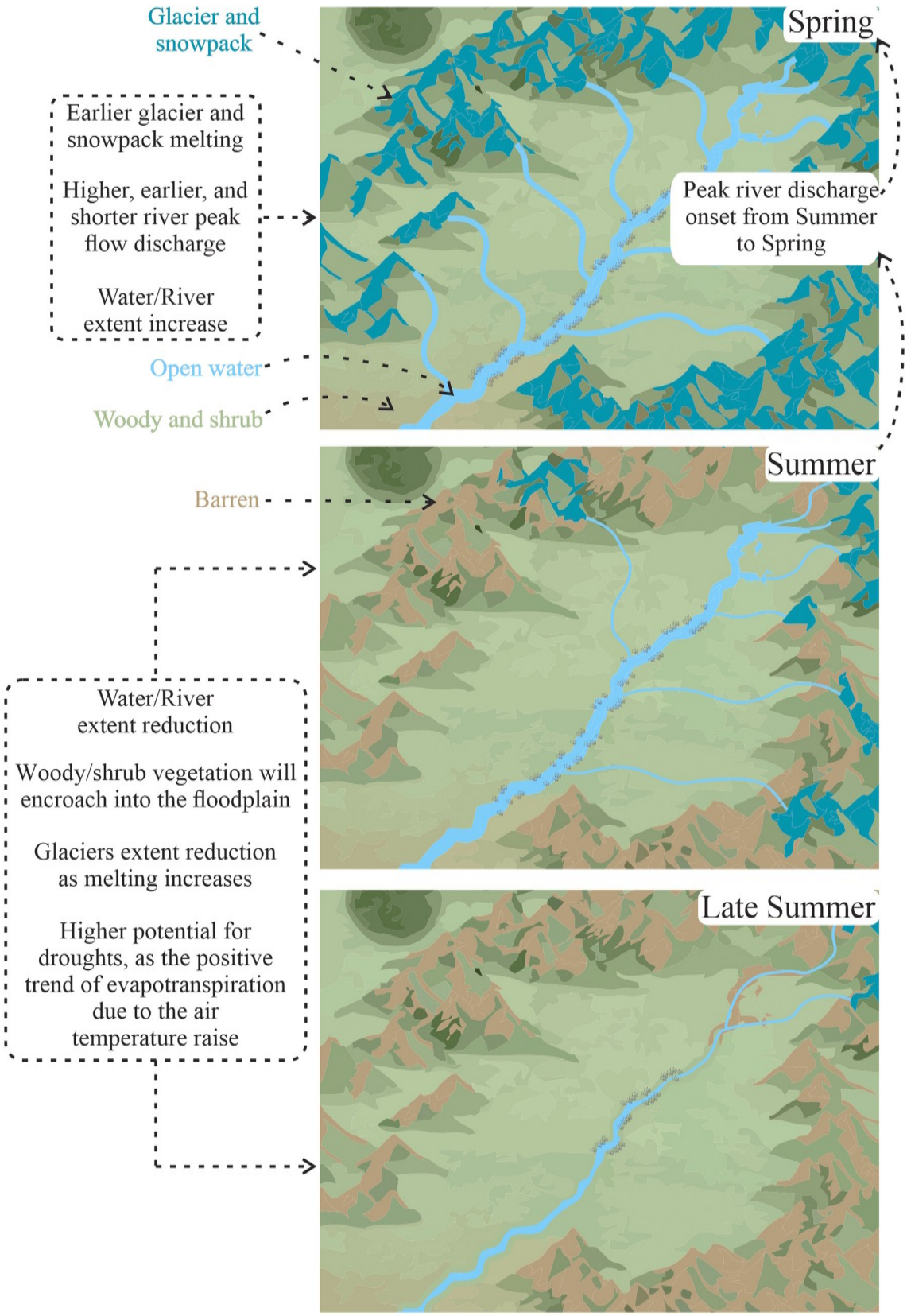

Fig. 12. Projected hydrological processes and land cover changes by season for the UCRW.

that are favorable for the seeds to land and germinate (Mahoney and Rood, 1998; Peters et al., 2015). Projected earlier peak discharge (in May or June instead of July) and flood pulse shrink can promote the seedling during summer season, since the cottonwood seedling occurs from May to July (Braatne et al., 1996) and they need exposes moist areas to germinate. However, in the late summer, reduced flow discharges may hinder the initial establishment of cottonwood seedlings at streambank elevations, leading to higher mortality rates among small seedlings (Rood et al., 1998). This is because the post-flood period is crucial for seedling recruitment (Rood et al., 2005; Polzin and Rood, 2006). However, projected increases in rainfall during the late summer could mitigate these adverse effects by raising soil moisture levels. Furthermore, the encroachment of woody shrubs may also impact water movement and the evapotranspiration (Cui et al., 2022), which may also lead to a decrease in soil moisture (Deng et al., 2021).

These projected changes described here may also affect the animals that live within the floodplain. Drier and more shrubby wetlands may be less hospitable for fish and amphibians, which may decline as the open water areas shrink (Hof et al., 2011). Climate-altered wetlands with less open water areas may also reduce the habitat for migratory waterbirds, as they use these wet regions on their way north or for reproduction (Haig et al., 2019). Furthermore, the habitat heterogeneity and interspersion of herbaceous, woody and shrub vegetation can impact the recruitment and establishment of cottonwood seedlings surrounded by herbaceous plant neighbors. This is because cottonwood seedlings are shade-intolerant (require full sunlight to grow) and experience negative impacts from adult conspecific neighbors, in this case, the herbaceous ones (Comita and Hubbell, 2009; Yin et al., 2023).

In summary, the projected changes for the UCRW include an increase in peak discharge of the Upper Columbia River and a shift in the peak open water area from summer to spring, and reduction by late summer (Fig. 12). The marsh areas are projected to decrease in all seasons. The wet meadow is projected to decrease in size throughout the spring, but it is expected to expand during the summer and late summer. Woody and shrub encroachment is projected to increase through all seasons.

5. Challenges and limitations of river discharge and LC projections

Multiple studies have identified uncertainties and ambiguity in regression models in accurately forecasting and predicting river flow in locations where snow processes play a significant role in driving the runoff and river discharge patterns (Alexander et al., 2016). The primary concern is around the timing of snowmelt in the future and the subsequent response and adaptation of the land and its biota to this shift. Utilising additional hydroclimatological factors, such as surface temperature, ground water, and shortwave or long wave radiation, have the potential to improve the accuracy of river discharge projections. Moreover, incorporating air temperature and total precipitation from previous months, such as February and March, could potentially enhance model performance, as river discharge reflects prior hydroclimatic conditions. Nonetheless, before spring and after late summer, only baseflow occurs (as per Rodrigues et al., 2024). Incorporating additional one or two months could potentially enhance the performance of hydroclimatic models by providing the model with more degrees of freedom. However, this improvement is likely attributable to the inclusion of periods with lower flows, which simplifies the estimation process.

Utilising GCMs to assess the potential effects of future climate change introduces additional uncertainty, as these models simulate several climatic scenarios known as RCPs. The objective of employing bias correction techniques is to minimise the discrepancy between model simulations and actual measurements within a specified reference period (in our case from 1984 to 2015). The validity of a bias correction strategy for the historical validation/reference period implies its continued validity for future periods (Zheng et al., 2019). This premise has garnered widespread acceptance in research on the effects of climate change (Fiseha et al., 2014; Kundzewicz et al., 2017; Teutschbein and Seibert, 2012).

The main uncertainty about artificial neural networks (ANN) is the only use of two-time steps, i.e., spatial land cover of the past (T1) and present (T2), to predict the future (T3), not allowing the use of other time steps between T1 and T2, which could theoretically improve learning. Nevertheless, terrain drivers enable the ANN to learn spatial correlations between land cover types and change throughout the floodplain, enhancing predictions (Gharaibeh et al., 2020). One potential method for improving the projections involves utilising additional time periods (for instance, T1 from 1984 to 1988, T2 from 1989 to 1993, to project T3, which spans 1994 to 1998, followed by assessing the accuracy of the projection against the reference dataset; thereafter, using T2 and T3 to estimate T4, covering 1999 to 2003, and so on), providing higher control over the projected land cover. However, the use of extra periods for land cover projections could lead to increased “trend noise”. This occurs as specific periods over time may primarily represent either dry or wet years, thereby affecting the land cover projections with a clear pattern (either wet or dry). Employing T1 (past) and T2 (present) aids in reducing the influence of trend noise. However, it is essential to ensure that both time points selected for the projections are representative periods, avoiding of any specific wet or dry conditions. The ANN algorithm in MOLUSCE is not flawless; however, it is generally more precise than other techniques for spatial land cover prediction (Gharaibeh et al., 2020; Ahmad et al., 2023). Ultimately, the ANN is consistent with the projected open water areas.

The higher uncertainty in the seasonal hydroclimatic models is (in theory) subject to their simplicity compared to full hydrological models (e.g., Raven hydrological modelling; Craig et al., 2020). Running a full hydrological model is intended to improve analysis, however seasonal parsimonious hydroclimatic models can be used in data-poor places such as montane regions. Finally, a comparison of the uncertainties of the hydroclimatic and full hydrological models would assist in determining whether the parsimonious model can accurately represent river discharge compared with a more complex model. This assessment would show the limit of when a more sophisticated or simpler model is valid.

Another factor that introduces uncertainty in the projections is the behaviour of animals, specifically beaver populations and beaver dams. Beaver dams may significantly expand the area of open water. For instance, it may be presumed that the increase in open water in the wetland is due to the faster melting of snow, however beavers, can play a crucial role in the local hydrology and often increase the area of open water in wetlands (Hood and Bayley, 2008; Hood and Larson, 2013).

6. Conclusion

This study employed an Artificial Neural Network (ANN) approach to evaluate linearly projected land-cover trends and changes (from 2020 to 2040) and compared against an independent open water projection for RCP 4.5 and 8.5 climate scenarios based on an empirical river discharge model in the Upper Columbia River Wetlands (UCRW). The ANN predicted land cover with a Kappa of 0.85 for 2020s comparing the reference and projected LC, and a Kappa of 0.82 for 2020s reference and projected LC change maps during the training phase. Significant changes were projected from 2020s to 2040s by the ANN, with a reduction of open water areas during late summer (August to mid-September), which are consistent with RCP 4.5 projections. Furthermore, the peak open water area in the UCRW is expected to transition from summer (late-May to July) to spring (April to mid-May) under both RCP scenarios. Rising air temperatures, with the anticipated associated changes to precipitation amounts, phase and earlier snowmelt, are projected to shift the Columbia River peak discharge from summer to spring under both RCP scenarios. Expected floodplain changes are a reduction in marsh area and increased wet meadow, particularly during summer and late summer. The area of woody/shrubs was projected to continue increasing

across all seasons which is aligned with a general trend of floodplain drying. Projected land cover trends using MOLUSCE assist in determining likely land cover gains and losses, and therefore can support mitigation measures to maintain ecological integrity or ecosystem services within the floodplain. Overall, the UCRW is projected to become greener (woody/shrub) and drier with less open water, especially during late summer.

CRediT authorship contribution statement

Italo Sampaio Rodrigues: Writing – review & editing, Writing – original draft, Validation, Methodology, Investigation, Formal analysis, Data curation, Conceptualization. **Christopher Hopkinson:** Writing – review & editing, Supervision, Software, Resources, Methodology, Investigation, Funding acquisition, Conceptualization. **Laura Chasmer:** Writing – review & editing, Supervision, Methodology, Investigation, Conceptualization. **Ryan J. MacDonald:** Writing – review & editing, Supervision, Conceptualization. **Suzanne E. Bayley:** Writing – review & editing, Supervision, Project administration, Investigation, Funding acquisition.

Declaration of competing interest

The authors declare that they have no known competing financial interests or personal relationships that could have appeared to influence the work reported in this paper.

Acknowledgements

The authors received funding from NSERC (grant no. 2017-04362), Alberta Innovates, the Nexen Fellowship in Water Resources, Columbia Wetlands Stewardship Partners, and the Shuswap Band's Columbia Headwaters Aquatic Restoration Secwépemc Strategy (CHARS) project.

Appendix A. Supplementary data

Supplementary data to this article can be found online at https://doi.org/10.1016/j.scitotenv.2024.178261.

Data availability

Data will be made available on request.

References

Aguirre, D., Benhumea, A.E., McLaren, J.R., 2020. Shrub encroachment affects tundra ecosystem properties through their living canopy rather than increased litter inputs. Soil Biol. Biochem. 153, 108121. https://doi.org/10.1016/j.soilbio.2020.108121.

Ahmad, H., Abdallah, M., Jose, F., Elzain, H.E., Bhuyan, M.S., Shoemaker, D.J., Selvam, S., 2023. Evaluation and mapping of predicted future land use changes using hybrid models in a coastal area. Eco. Inform. 78, 102324. https://doi.org/10.1016/j.ecoinf.2023.102324.

Alam, N., Saha, S., Gupta, S., Chakraborty, S., 2021. Prediction modelling of riverine landscape dynamics in the context of sustainable management of floodplain: a geospatial approach. Ann. GIS 27 (3), 299–314. https://doi.org/10.1080/19475683.2020.1870558.

Alexander, P., Prestele, R., Verburg, P.H., Arneth, A., Baranzelli, C., Silva, F.B.E., Brown, C., Butler, A., Calvin, K., Dendoncker, N., Doelman, J.C., Dunford, R., Engström, K., Eitelberg, D., Fujimori, S., Harrison, P.A., Hasegawa, T., Havlik, P., Holzhauer, S., Rounsevell, M.D.A., 2016. Assessing uncertainties in land cover projections. Glob. Chang. Biol. 23 (2), 767–781. https://doi.org/10.1111/gcb.13447.

Alshari, E.A., Gawali, B.W., 2022. Modeling land use change in Sana'a City of Yemen with MOLUSCE. J. Sens. 2022, 1–15. https://doi.org/10.1155/2022/7419031.

Althoff, D., Rodrigues, L.N., Da Silva, D.D., 2020. Impacts of climate change on the evaporation and availability of water in small reservoirs in the Brazilian savannah. Clim. Chang. 159 (2), 215–232. https://doi.org/10.1007/s10584-020-02656-y.

Amani, M., Mahdavi, S., Kakooei, M., Ghorbanian, A., Brisco, B., DeLancey, E., Toure, S., Reyes, E.L., 2021. Wetland change analysis in Alberta, Canada using four decades of Landsat imagery. IEEE J. Sel. Top. Appl. Earth Observ. Remote Sens. 14, 10314–10335. https://doi.org/10.1109/jstars.2021.3110460.

Bach, A.F., Van Der Schrier, G., Melsen, L.A., Tank, A.M.G.K., Teuling, A.J., 2018. Widespread and accelerated decrease of observed mean and extreme snow depth over Europe. Geophys. Res. Lett. 45 (22). https://doi.org/10.1029/2018gl079799.

Barnett, T.P., Adam, J.C., Lettenmaier, D.P., 2005. Potential impacts of a warming climate on water availability in snow-dominated regions. Nature 438 (7066), 303–309. https://doi.org/10.1038/nature04141.

Bates, B.C., Kundzewicz, Z.W., Wu, S., Arnell, N., Burgett, V., Räisänen, J., 2008. Climate Change and Water: Technical Paper of the Intergovernmental Panel on Climate Change. IPCC Secretariat, Geneva. https://researchportal.helsinki.fi/sv/publications/climate-change-and-water-technical-paper-of-the-intergovernmental.

Bjørnæs, C., 2013. A Guide to Representative Concentration Pathways. CICERO. Center for International Climate and Environmental Research, pp. 351–357.

Bolch, T., Menounos, B., Wheate, R., 2010. Landsat-based inventory of glaciers in western Canada, 1985–2005. Remote Sens. Environ. 114 (1), 127–137. https://doi.org/10.1016/j.rse.2009.08.015.

Booij, M.J., 2004. Impact of climate change on river flooding assessed with different spatial model resolutions. J. Hydrol. 303 (1–4), 176–198. https://doi.org/10.1016/j.jhydrol.2004.07.013.

Braatne, J.H., Rood, S.B., Heilman, P.E., 1996. Life history, ecology, and conservation of riparian cottonwoods in North America. In: Biology of Populus and its Implications for Management and Conservation (Part I), pp. 57–85.

Brinson, M.M., Malvárez, A.I., 2002. Temperate freshwater wetlands: types, status, and threats. Environ. Conserv. 29 (2), 115–133. https://doi.org/10.1017/s0376892902000085.

Bürger, G., Schulla, J., Werner, A.T., 2011. Estimates of future flow, including extremes, of the Columbia River headwaters. Water Resour. Res. 47 (10). https://doi.org/10.1029/2010wr009716.

Carli, C.M., Bayley, S.E., 2015. River connectivity and road crossing effects on floodplain vegetation of the upper Columbia River, Canada. Ecoscience 22 (2–4), 97–107. https://doi.org/10.1080/11956860.2015.1121705.

Carver, M., 2017. Water Monitoring and Climate Change in the Upper Columbia Basin: Summary of Current Status and Opportunities. Columbia Basin Trust, Castlegar, BC, Canada.

Chatterjee, A., Blom, E., Gujja, B., Jacimovic, R., Beevers, L., O'Keeffe, J., Beland, M., Biggs, T., 2010. WWF initiatives to study the impact of climate change on Himalayan high-altitude wetlands (HAWs). Mt. Res. Dev. 30 (1), 42–52. https://doi.org/10.1659/mrd-journal-d-09-00091.1.

Chen, J., Brissette, F.P., Chaumont, D., Braun, M., 2013. Finding appropriate bias correction methods in downscaling precipitation for hydrologic impact studies over North America. Water Resour. Res. 49 (7), 4187–4205. https://doi.org/10.1002/wrcr.20331.

Clair, T.A., Warner, B.G., Robarts, R., Murkin, H., Lilley, J., Mortsch, L., Avis, W., 1998. Canadian inland wetlands and climate change. In: The Canada Country Study: Climate Impacts and Adaptation. National Sectoral Volume. Environment Canada, Ottawa, Ontario, Canada, pp. 189–218.

Clarke, G.K.C., Jarosch, A.H., Anslow, F.S., Radić, V., Menounos, B., 2015. Projected deglaciation of western Canada in the twenty-first century. Nat. Geosci. 8 (5), 372–377. https://doi.org/10.1038/ngeo2407.

Comita, L.S., Hubbell, S.P., 2009. Local neighborhood and species' shade tolerance influence survival in a diverse seedling bank. Ecology 90 (2), 328–334. https://doi.org/10.1890/08-0451.1.

Cooper, D.J., Kaczynski, K.M., Sueltenfuss, J., Gaucherand, S., Hazen, C., 2017. Mountain wetland restoration: the role of hydrologic regime and plant introductions after 15 years in the Colorado Rocky Mountains, USA. Ecol. Eng. 101, 46–59. https://doi.org/10.1016/j.ecoleng.2017.01.017.

Craig, J.R., Brown, G., Chlumsky, R., Jenkinson, R.W., Jost, G., Lee, K., Mai, J., Serrer, M., Sgro, N., Shafii, M., Snowdon, A.P., Tolson, B.A., 2020. Flexible watershed simulation with the raven hydrological modelling framework. Environ. Model Softw. 129, 104728. https://doi.org/10.1016/j.envsoft.2020.104728.

Cui, J., Lian, X., Huntingford, C., Gimeno, L., Wang, T., Ding, J., He, M., Xu, H., Chen, A., Gentine, P., Piao, S., 2022. Global water availability boosted by vegetation-driven changes in atmospheric moisture transport. Nat. Geosci. 15 (12), 982–988. https://doi.org/10.1038/s41561-022-01061-7.

De Reu, J., Bourgeois, J., Bats, M., Zwertvaegher, A., Gelorini, V., De Smedt, P., Chu, W., Antrop, M., De Maeyer, P., Finke, P., Van Meirvenne, M., Verniers, J., Crombé, P., 2012. Application of the topographic position index to heterogeneous landscapes. Geomorphology 186, 39–49. https://doi.org/10.1016/j.geomorph.2012.12.015.

DeBeer, C.M., Wheater, H.S., Carey, S.K., Chun, K.P., 2015. Recent climatic, cryospheric, and hydrological changes over the interior of western Canada: a synthesis and review. Hydrol. Earth Syst. Sci. https://doi.org/10.5194/hessd-12-8615-2015.

DeBeer, C.M., Wheater, H.S., Pomeroy, J.W., Barr, A.G., Baltzer, J.L., Johnstone, J.F., Turetsky, M.R., Stewart, R.E., Hayashi, M., Van Der Kamp, G., Marshall, S., Campbell, E., Marsh, P., Carey, S.K., Quinton, W.L., Li, Y., Razavi, S., Berg, A., McDonnell, J.J., Pietroniro, A., 2021. Summary and synthesis of Changing Cold Regions Network (CCRN) research in the interior of western Canada — part 2: future change in cryosphere, vegetation, and hydrology. Hydrol. Earth Syst. Sci. 25 (4), 1849–1882. https://doi.org/10.5194/hess-25-1849-2021.

Deng, Y., Li, X., Shi, F., Hu, X., 2021. Woody plant encroachment enhanced global vegetation greening and ecosystem water-use efficiency. Glob. Ecol. Biogeogr. 30 (12), 2337–2353. https://doi.org/10.1111/geb.13386.

Díaz, S., Demissew, S., Carabias, J., Joly, C., Lonsdale, M., Ash, N., Larigauderie, A., Adhikari, J.R., Arico, S., Báldi, A., Bartuska, A., Baste, I.A., Bilgin, A., Brondizio, E., Chan, K.M., Figueroa, V.E., Duraiappah, A., Fischer, M., Hill, R., Zlatanova, D., 2014. The IPBES Conceptual Framework — connecting nature and people. Curr. Opin. Environ. Sustain. 14, 1–16. https://doi.org/10.1016/j.cosust.2014.11.002.

Diomede, T., Davolio, S., Marsigli, C., Miglietta, M.M., Moscatello, A., Papetti, P., Paccagnella, T., Buzzi, A., Malguzzi, P., 2008. Discharge prediction based on multi-model precipitation forecasts. Meteorog. Atmos. Phys. 101 (3–4), 245–265. https://doi.org/10.1007/s00703-007-0285-0.

Edwards, T.W., Birks, S.J., Luckman, B.H., MacDonald, G.M., 2008. Climatic and hydrologic variability during the past millennium in the eastern Rocky Mountains and northern Great Plains of western Canada. Quat. Res. 70 (2), 188–197. https://doi.org/10.1016/j.yqres.2008.04.013.

Environment and Climate Change Canada/Environnement et Changement Climatique Canada, 2021. CMIP6 ensemble of daily predictor variables (Version 1) [Dataset]. In: Canadian Climate Data and Scenarios. https://climate-scenarios.canada.ca/?page=pred-cmip6.

Environment Canada, 2022a. Historical Climate Data. Environment Canada. Accessed November, 2022. https://climate.weather.gc.ca/historical_data/search_historic_data_e.html.

Environment Canada, 2022b. HYDAT Database. Environment Canada. Accessed November, 2022. https://wateroffice.ec.gc.ca/search/historical_e.html.

Environment Canada, 2022c. HYDAT Database. Environment Canada. Accessed November, 2023. https://wateroffice.ec.gc.ca/report/historical_e.html?stn=08NA002.

Fischenich, J.C., Copeland, R.R., 2001. Environmental considerations for vegetation in flood control channels. This Digital Resource was created in Microsoft Word and Adobe Acrobat. https://erdc-library.erdc.dren.mil/jspui/bitstream/11681/8536/1/12654.pdf.

Fiseha, B., Setegn, S., Melesse, A., Volpi, E., Fiori, A., 2014. Impact of climate change on the hydrology of Upper Tiber River Basin using bias corrected regional climate model. Water Resour. Manag. 28 (5), 1327–1343. https://doi.org/10.1007/s11269-014-0546-x.

Flannigan, M.D., Krawchuk, M.A., de Groot, W.J., Wotton, B.M., Gowman, L.M., 2009. Implications of changing climate for global wildland fire. Int. J. Wildland Fire 18 (5), 483–507. https://doi.org/10.1071/WF08187.

Fleming, S.W., Dahlke, H.E., 2014. Modulation of linear and nonlinear hydroclimatic dynamics by mountain glaciers in Canada and Norway: results from information-theoretic polynomial selection. Can. Water Resour. J./Rev. Can. Ressour. Hydriq. 39 (3), 324–341. https://doi.org/10.1080/07011784.2014.942164.

Formica, A., Farrer, E.C., Ashton, I.W., Suding, K.N., 2014. Shrub expansion over the past 62 years in Rocky Mountain alpine tundra: possible causes and consequences. Arct. Antarct. Alp. Res. 46 (3), 616–631. https://doi.org/10.1657/1938-4246-46.3.616.

Gašparović, M., Jogun, T., 2017. The effect of fusing Sentinel-2 bands on land-cover classification. Int. J. Remote Sens. 39 (3), 822–841. https://doi.org/10.1080/01431161.2017.1392640.

Gharaibeh, A., Shaamala, A., Obeidat, R., Al-Kofahi, S., 2020. Improving land-use change modeling by integrating ANN with Cellular Automata-Markov Chain model. Heliyon 6 (9), e05092. https://doi.org/10.1016/j.heliyon.2020.e05092.

Girardin, M.P., Tardif, J.C., Flannigan, M.D., Bergeron, Y., 2006. Forest fire-conducive drought variability in the southern Canadian boreal forest and associated climatology inferred from tree rings. Can. Water Resour. J./Rev. Can. Ressour. Hydriq. 31 (4), 275–296. https://doi.org/10.4296/cwrj3104275.

Glines, L.M., 2012. Woody Plant Encroachment Into Grasslands Within the Red Deer River Drainage, Alberta. ERA: Education and Research Archive. https://doi.org/10.7939/r33h5v.

Gomes, L., Bianchi, F., Cardoso, I., Schulte, R., Arts, B., Filho, E.F., 2020. Land use and land cover scenarios: an interdisciplinary approach integrating local conditions and the global shared socioeconomic pathways. Land Use Policy 97, 104723. https://doi.org/10.1016/j.landusepol.2020.104723.

Haig, S.M., Murphy, S.P., Matthews, J.H., Arismendi, I., Safeeq, M., 2019. Climate-altered wetlands challenge waterbird use and migratory connectivity in arid landscapes. Sci. Rep. 9 (1). https://doi.org/10.1038/s41598-019-41135-y.

Hamlet, A.F., Elsner, M.M., Mauger, G.S., Lee, S., Tohver, I., Norheim, R.A., 2013. An overview of the Columbia Basin climate change scenarios project: approach, methods, and summary of key results. Atmosphere Ocean 51 (4), 392–415. https://doi.org/10.1080/07055900.2013.819555.

Harrington, J., Flannigan, M., 1993. A model for the frequency of long periods of drought at forested stations in Canada. J. Appl. Meteorol. 32 (11), 1708–1716. https://doi.org/10.1175/1520-0450(1993)032.

Hof, C., Araújo, M.B., Jetz, W., Rahbek, C., 2011. Additive threats from pathogens, climate and land-use change for global amphibian diversity. Nature 480 (7378), 516–519. https://doi.org/10.1038/nature10650.

Hood, G.A., Bayley, S.E., 2008. Beaver (*Castor canadensis*) mitigate the effects of climate on the area of open water in boreal wetlands in western Canada. Biol. Conserv. 141 (2), 556–567. https://doi.org/10.1016/j.biocon.2007.12.003.

Hood, G.A., Larson, D.G., 2013. Beaver-created habitat heterogeneity influences aquatic invertebrate assemblages in boreal Canada. Wetlands 34 (1), 19–29. https://doi.org/10.1007/s13157-013-0476-z.

Hopkinson, C., Fuoco, B., Grant, T., Bayley, S.E., Brisco, B., MacDonald, R., 2020. Wetland hydroperiod change along the upper Columbia River floodplain, Canada, 1984 to 2019. Remote Sens. 12 (24), 4084. https://doi.org/10.3390/rs12244084.

Hrach, D.M., Petrone, R.M., Green, A., Khomik, M., 2022. Analysis of growing season carbon and water fluxes of a subalpine wetland in the Canadian Rocky Mountains: implications of shade on ecosystem water use efficiency. Hydrol. Process. 36 (1), e14425.

Hussain, M., Mahmud, I., 2019. pyMannKendall: a python package for non parametric Mann Kendall family of trend tests. J. Open Source Softw. 4 (39), 1556. https://doi.org/10.21105/joss.01556.

Johnson, W.C., Millett, B.V., Gilmanov, T., Voldseth, R.A., Guntenspergen, G.R., Naugle, D.E., 2005. Vulnerability of northern prairie wetlands to climate change. BioScience 55 (10), 863. https://doi.org/10.1641/0006-3568(2005)055.

Jost, G., Moore, R.D., Menounos, B., Wheate, R., 2012. Quantifying the contribution of glacier runoff to streamflow in the upper Columbia River Basin, Canada. Hydrol. Earth Syst. Sci. 16 (3), 849–860. https://doi.org/10.5194/hess-16-849-2012.

Kamaraj, M., Rangarajan, S., 2022. Predicting the future land use and land cover changes for Bhavani basin, Tamil Nadu, India, using QGIS MOLUSCE plugin. Environ. Sci. Pollut. Res. 29 (57), 86337–86348. https://doi.org/10.1007/s11356-021-17904-6.

Keddy, P., Reznicek, A., 1986. Great lakes vegetation dynamics: the role of fluctuating water levels and buried seeds. J. Great Lakes Res. 12 (1), 25–36. https://doi.org/10.1016/s0380-1330(86)71697-3.

Keddy, P.A., 2011. Wetland ecology: principles and conservation. Choice Rev. Online 48 (08), 48–4471. https://doi.org/10.5860/choice.48-4471.

Kendall, M.G., 1957. Rank correlation methods. Biometrika 44 (1/2), 298. https://doi.org/10.2307/2333282.

Kienzle, S.W., 2006. The use of the recession index as an indicator for streamflow recovery after a multi-year drought. Water Resour. Manag. 20 (6), 991–1006. https://doi.org/10.1007/s11269-006-9019-1.

Knowles, N., Dettinger, M.D., Cayan, D.R., 2006. Trends in snowfall versus rainfall in the Western United States. J. Clim. 19 (18), 4545–4559. https://doi.org/10.1175/jcli3850.1.

Kołos, A., Banaszuk, P., 2013. Mowing as a tool for wet meadows restoration: effect of long-term management on species richness and composition of sedge-dominated wetland. Ecol. Eng. 55, 23–28. https://doi.org/10.1016/j.ecoleng.2013.02.008.

Koomen, E., Beurden, J.B., 2011. Land-use Modelling in Planning Practice. Springer Science & Business Media.

Kundzewicz, Z., Krysanova, V., Benestad, R., Hov, Ø., Piniewski, M., Otto, I., 2017. Uncertainty in climate change impacts on water resources. Environ. Sci. Pol. 79, 1–8. https://doi.org/10.1016/j.envsci.2017.10.008.

Lau, K.H., Kam, B.H., 2005. A cellular automata model for urban land-use simulation. Environ. Plann. B Plann. Des. 32 (2), 247–263. https://doi.org/10.1068/b31110.

Leipe, S.C., Carey, S.K., 2021. Rapid shrub expansion in a subarctic mountain basin revealed by repeat airborne LiDAR. Environ. Res. Commun. 3 (7), 071001. https://doi.org/10.1088/2515-7620/ac0e0c.

Levenberg, K., 1944. A method for the solution of certain non-linear problems in least squares. Q. Appl. Math. 2 (2), 164–168. https://doi.org/10.1090/qam/10666.

Li, K., Coe, M., Ramankutty, N., De Jong, R., 2007. Modeling the hydrological impact of land-use change in West Africa. J. Hydrol. 337 (3–4), 258–268. https://doi.org/10.1016/j.jhydrol.2007.01.038.

Löffler, J., Anschlag, K., Baker, B., Finch, O., Wundram, D., Diekkrüger, B., Schröder, B., Pape, R., Lundberg, A., 2011. Mountain ecosystem response to global change. Erdkunde 65 (2), 189–213. https://doi.org/10.3112/erdkunde.2011.02.06.

Lottig, N.R., Buffam, I., Stanley, E.H., 2013. Comparisons of wetland and drainage lake influences on stream dissolved carbon concentrations and yields in a north temperate lake-rich region. Aquat. Sci. 75 (4), 619–630. https://doi.org/10.1007/s00027-013-0305-8.

MacDonald, R.J., Byrne, J.M., Kienzle, S.W., Larson, R.P., 2010. Assessing the potential impacts of climate change on mountain snowpack in the St. Mary River Watershed, Montana. J. Hydrometeorol. 12 (2), 262–273. https://doi.org/10.1175/2010jhm1294.1.

Mahoney, J.M., Rood, S.B., 1998. Streamflow requirements for cottonwood seedling recruitment—an integrative model. Wetlands 18 (4), 634–645. https://doi.org/10.1007/bf03161678.

Mann, H.B., 1945. Nonparametric tests against trend. Econometrica 13 (3), 245. https://doi.org/10.2307/1907187.

Marquardt, D.W., 1963. An algorithm for least-squares estimation of nonlinear parameters. J. Soc. Ind. Appl. Math. 11 (2), 431–441. https://doi.org/10.1137/0111030.

McClymont, A.F., Hayashi, M., Bentley, L.R., Muir, D., Ernst, E., 2010. Groundwater flow and storage within an alpine meadow-talus complex. Hydrol. Earth Syst. Sci. 14 (6), 859–872. https://doi.org/10.5194/hess-14-859-2010.

Middelkoop, H., Daamen, K., Gellens, D., Grabs, W., Kwadijk, J.C.J., Lang, H., Parmet, B. W.H., Schädler, B., Schulla, J., Wilke, K., 2001. Impact of climate change on hydrological regimes and water resources management in the Rhine Basin. Clim. Chang. 49 (1/2), 105–128. https://doi.org/10.1023/a:1010784727448.

Milly, P.C.D., Dunne, K.A., Vecchia, A.V., 2005. Global pattern of trends in streamflow and water availability in a changing climate. Nature 438 (7066), 347–350. https://doi.org/10.1038/nature04312.

Milner, A.M., Khamis, K., Battin, T.J., Brittain, J.E., Barrand, N.E., Füreder, L., Cauvy-Fraunié, S., Gíslason, G.M., Jacobsen, D., Hannah, D.M., Hodson, A.J., Hood, E., Lencioni, V., Ólafsson, J.S., Robinson, C.T., Tranter, M., Brown, L.E., 2017. Glacier shrinkage driving global changes in downstream systems. Proc. Natl. Acad. Sci. 114 (37), 9770–9778. https://doi.org/10.1073/pnas.1619807114.

Mirmasoudi, S., Byrne, J., MacDonald, R., Johnson, D., Kroebel, R., 2019. Modelling historical and potential future climate impacts on Keremeos Creek, an Okanagan-Similkameen watershed, British Columbia, Canada: part I. Forecasting change in spring and summer water supply and demand. Can. Water Resour. J./Rev. Can. Ressour. Hydriq. 44 (4), 350–366. https://doi.org/10.1080/07011784.2019.1640137.

Moore, R.D., Fleming, S.W., Menounos, B., Wheate, R., Fountain, A., Stahl, K., Holm, K., Jakob, M., 2008. Glacier change in western North America: influences on hydrology, geomorphic hazards and water quality. Hydrol. Process. 23 (1), 42–61. https://doi.org/10.1002/hyp.7162.

Moore, R.D., Pelto, B., Menounos, B., Hutchinson, D., 2020. Detecting the effects of sustained glacier wastage on streamflow in variably glacierized catchments. Front. Earth Sci. 8. https://doi.org/10.3389/feart.2020.00136.

Moradkhani, H., Baird, R.G., Wherry, S.A., 2010. Assessment of climate change impact on floodplain and hydrologic ecotones. J. Hydrol. 395 (3–4), 264–278. https://doi.org/10.1016/j.jhydrol.2010.10.038.

Moser, K., Baron, J., Brahney, J., Oleksy, I., Saros, J., Hundey, E., Sadro, S., Kopáček, J., Sommaruga, R., Kainz, M., Strecker, A., Chandra, S., Walters, D., Preston, D., Michelutti, N., Lepori, F., Spaulding, S., Christianson, K., Melack, J., Smol, J., 2019. Mountain lakes: eyes on global environmental change. Glob. Planet. Chang. 178, 77–95. https://doi.org/10.1016/j.gloplacha.2019.04.001.

Muhammad, R., Zhang, W., Abbas, Z., Guo, F., Gwiazdzinski, L., 2022. Spatiotemporal change analysis and prediction of future land use and land cover changes using QGIS MOLUSCE plugin and remote sensing big data: a case study of Linyi, China. Land 11 (3), 419. https://doi.org/10.3390/land11030419.

Nash, J., Sutcliffe, J., 1970. River flow forecasting through conceptual models part I — A discussion of principles. J. Hydrol. 10 (3), 282–290. https://doi.org/10.1016/0022-1694(70)90255-6.

NextGIS, 2017. MOLUSCE-quick and convenient aanalysis of Land-Cover Changes. https://nextgis.com/blog/molusce/ (accessed 25 February 2023).

Nohara, D., Kitoh, A., Hosaka, M., Oki, T., 2006. Impact of climate change on river discharge projected by multimodel ensemble. J. Hydrometeorol. 7 (5), 1076–1089. https://doi.org/10.1175/jhm531.1.

Peters, D., Caissie, D., Monk, W., Rood, S., St-Hilaire, A., 2015. An ecological perspective on floods in Canada. Can. Water Resour. J./Rev. Can. Ressour. Hydriq. 41 (1–2), 288–306. https://doi.org/10.1080/07011784.2015.1070694.

Polzin, M.L., Rood, S.B., 2006. Effective disturbance: seedling safe sites and patch recruitment of riparian cottonwoods after a major flood of a mountain river. Wetlands 26 (4), 965–980. https://doi.org/10.1672/0277-5212(2006)26.

Rahman, M.T.U., Tabassum, F., Rasheduzzaman, M., Saba, H., Sarkar, L., Ferdous, J., Uddin, S.Z., Islam, A.Z.M.Z., 2017. Temporal dynamics of land use/land cover change and its prediction using CA-ANN model for southwestern coastal Bangladesh. Environ. Monit. Assess. 189 (11). https://doi.org/10.1007/s10661-017-6272-0.

Rodrigues, I.S., Hopkinson, C., Chasmer, L., MacDonald, R.J., Bayley, S.E., Brisco, B., 2024. Multi-decadal floodplain classification and trend analysis in the Upper Columbia River valley, British Columbia. Hydrol. Earth Syst. Sci. 28 (10), 2203–2221. https://doi.org/10.5194/hess-28-2203-2024.

Rood, S.B., Kalischuk, A.R., Mahoney, J.M., 1998. Initial cottonwood seedling recruitment following the flood of the century of the Oldman River, Alberta, Canada. Wetlands 18 (4), 557–570. https://doi.org/10.1007/bf03161672.

Rood, S.B., Braatne, J.H., Hughes, F.M.R., 2003. Ecophysiology of riparian cottonwoods: stream flow dependency, water relations and restoration. Tree Physiol. 23 (16), 1113–1124. https://doi.org/10.1093/treephys/23.16.1113.

Rood, S.B., Samuelson, G.M., Braatne, J.H., Gourley, C.R., Hughes, F.M., Mahoney, J.M., 2005. Managing river flows to restore floodplain forests. Front. Ecol. Environ. 3 (4), 193–201. https://doi.org/10.1890/1540-9295(2005)003[0193:MRFTRF]2.0.CO;2.

Rooney, R.C., Carli, C., Bayley, S.E., 2013. River connectivity affects submerged and floating aquatic vegetation in floodplain wetlands. Wetlands 33 (6), 1165–1177. https://doi.org/10.1007/s13157-013-0471-4.

Schnorbus, M., Werner, A., Bennett, K., 2012. Impacts of climate change in three hydrologic regimes in British Columbia, Canada. Hydrol. Process. 28 (3), 1170–1189. https://doi.org/10.1002/hyp.9661.

Shrestha, M., Acharya, S.C., Shrestha, P.K., 2017. Bias correction of climate models for hydrological modelling — are simple methods still useful? Meteorol. Appl. 24 (3), 531–539. https://doi.org/10.1002/met.1655.

Silva, W.P.D., Silva, C.M., Cavalcanti, C.G., Silva, D.D., Soares, I.B., Oliveira, J.A., Silva, C.D., 2004. LAB fit curve fitting: a software in portuguese for treatment of experimental data. Rev. Bras. Ens. Fís. 26, 419–427. https://doi.org/10.1590/S1806-11172004000400018.

Sparks, R.E., 1995. Need for ecosystem management of large rivers and their floodplains. BioScience 45 (3), 168–182. https://doi.org/10.2307/1312556.

Stahl, K., Moore, R.D., 2006. Influence of watershed glacier coverage on summer streamflow in British Columbia, Canada. Water Resour. Res. 42 (6). https://doi.org/10.1029/2006wr005022.

Steiger, J., Tabacchi, E., Dufour, S., Corenblit, D., Peiry, J.L., 2005. Hydrogeomorphic processes affecting riparian habitat within alluvial channel–floodplain river systems: a review for the temperate zone. River Res. Appl. 21 (7), 719–737. https://doi.org/10.1002/rra.879.

Stewart, I.T., 2009. Changes in snowpack and snowmelt runoff for key mountain regions. Hydrol. Process. 23 (1), 78–94. https://doi.org/10.1002/hyp.7128.

Stewart, I.T., Cayan, D.R., Dettinger, M.D., 2005. Changes toward earlier streamflow timing across Western North America. J. Clim. 18 (8), 1136–1155. https://doi.org/10.1175/jcli3321.1.

Swart, N.C., Cole, J.N., Kharin, V.V., Lazare, M., Scinocca, J.F., Gillett, N.P., Winter, B., 2019. The Canadian earth system model version 5 (CanESM5.0.3). Geosci. Model Dev. 12 (11), 4823–4873. https://doi.org/10.5194/gmd-12-4823-2019.

Teuling, A.J., De Badts, E.G., Jansen, F.A., Fuchs, R., Buitink, J., Van Dijke, A.J.H., Sterling, S.M., 2019. Climate change, reforestation/afforestation, and urbanization impacts on evapotranspiration and streamflow in Europe. Hydrol. Earth Syst. Sci. 23 (9), 3631–3652. https://doi.org/10.5194/hess-23-3631-2019.

Teutschbein, C., Seibert, J., 2012. Bias correction of regional climate model simulations for hydrological climate-change impact studies: review and evaluation of different methods. J. Hydrol. 456–457, 12–29. https://doi.org/10.1016/j.jhydrol.2012.05.052.

Thomson, A.M., Calvin, K.V., Smith, S.J., Kyle, G.P., Volke, A., Patel, P., Delgado-Arias, S., Bond-Lamberty, B., Wise, M.A., Clarke, L.E., Edmonds, J.A., 2011. RCP4.5: a pathway for stabilization of radiative forcing by 2100. Clim. Chang. 109 (1–2), 77–94. https://doi.org/10.1007/s10584-011-0151-4.

Tsuruta, K., Schnorbus, M.A., 2021. Exploring the operational impacts of climate change and glacier loss in the upper Columbia River Basin, Canada. Hydrol. Process. 35 (7). https://doi.org/10.1002/hyp.14253.

Van Der Valk, A.G., 2005. Water-level fluctuations in North American prairie wetlands. Hydrobiologia 539 (1), 171–188. https://doi.org/10.1007/s10750-004-4866-3.

VanShaar, J.R., Haddeland, I., Lettenmaier, D.P., 2002. Effects of land-cover changes on the hydrological response of interior Columbia River basin forested catchments. Hydrol. Process. 16 (13), 2499–2520. https://doi.org/10.1002/hyp.1017.

Wang, W.Y., Wang, Q.J., Wang, C.Y., Shi, H.L., Li, Y., Wang, G., 2005. The effect of land management on carbon and nitrogen status in plants and soils of alpine meadows on the Tibetan Plateau. Land Degrad. Dev. 16 (5), 405–415. https://doi.org/10.1002/ldr.661.

Wang, X., Parisien, M., Taylor, S.W., Candau, J., Stralberg, D., Marshall, G.A., Little, J. M., Flannigan, M.D., 2017. Projected changes in daily fire spread across Canada over the next century. Environ. Res. Lett. 12 (2), 025005. https://doi.org/10.1088/1748-9326/aa5835.

Wang, X., Studens, K., Parisien, M., Taylor, S.W., Candau, J., Boulanger, Y., Flannigan, M.D., 2020. Projected changes in fire size from daily spread potential in Canada over the 21st century. Environ. Res. Lett. 15 (10), 104048. https://doi.org/10.1088/1748-9326/aba101.

Weiland, F.C.S., Van Beek, L.P.H., Kwadijk, J.C.J., Bierkens, M.F.P., 2012. Global patterns of change in discharge regimes for 2100. Hydrol. Earth Syst. Sci. 16 (4), 1047–1062. https://doi.org/10.5194/hess-16-1047-2012.

Werner, A.T., Schnorbus, M.A., Shrestha, R.R., Eckstrand, H.D., 2013. Spatial and temporal change in the hydro-climatology of the Canadian portion of the Columbia River basin under multiple emissions scenarios. Atmos. Ocean 51 (4), 357–379. https://doi.org/10.1080/07055900.2013.821400.

Williamson, C.E., Dodds, W., Kratz, T.K., Palmer, M.A., 2008. Lakes and streams as sentinels of environmental change in terrestrial and atmospheric processes. Front. Ecol. Environ. 6 (5), 247–254. https://doi.org/10.1890/070140.

Wulder, M.A., Roy, D.P., Radeloff, V.C., Loveland, T.R., Anderson, M.C., Johnson, D.M., Healey, S., Zhu, Z., Scambos, T.A., Pahlevan, N., Hansen, M., Gorelick, N., Crawford, C.J., Masek, J.G., Hermosilla, T., White, J.C., Belward, A.S., Schaaf, C., Woodcock, C.E., Cook, B.D., 2022. Fifty years of Landsat science and impacts. Remote Sens. Environ. 280, 113195. https://doi.org/10.1016/j.rse.2022.113195.

Yatoo, S.A., Sahu, P., Kalubarme, M.H., Kansara, B.B., 2020. Monitoring land use changes and its future prospects using cellular automata simulation and artificial neural network for Ahmedabad city, India. GeoJournal 87 (2), 765–786. https://doi.org/10.1007/s10708-020-10274-5.

Yin, Z., Zhang, C., Fan, X., Zhang, N., Zhao, X., Von Gadow, K., 2023. Effects of tree density and herbaceous plants on tree seedling survival across the growing and non-growing season in a temperate forest. For. Ecol. Manag. 545, 121234. https://doi.org/10.1016/j.foreco.2023.121234.

Zhang, H., Huang, G.H., Wang, D., Zhang, X., 2011. Multi-period calibration of a semi-distributed hydrological model based on hydroclimatic clustering. Adv. Water Resour. 34 (10), 1292–1303. https://doi.org/10.1016/j.advwatres.2011.06.005.

Zhang, L., Wang, X., Wang, J., Liao, L., Lei, S., Liu, G., Zhang, C., 2022b. Alpine meadow degradation depresses soil nitrogen fixation by regulating plant functional groups and diazotrophic community composition. Plant Soil 473 (1–2), 319–335. https://doi.org/10.1007/s11104-021-05287-z.

Zhang, T., Li, D., East, A.E., Walling, D.E., Lane, S., Overeem, I., Beylich, A.A., Koppes, M., Lu, X., 2022a. Warming-driven erosion and sediment transport in cold regions. Nat. Rev. Earth Environ. 1–20. https://doi.org/10.1038/s43017-022-00362-0.

Zheng, J., Wang, W., Ding, Y., Liu, G., Xing, W., Cao, X., Chen, D., 2019. Assessment of climate change impact on the water footprint in rice production: historical simulation and future projections at two representative rice cropping sites of China. Sci. Total Environ. 709, 136190. https://doi.org/10.1016/j.scitotenv.2019.136190.

Zwieback, S., Chang, Q., Marsh, P., Berg, A., 2019. Shrub tundra ecohydrology: rainfall interception is a major component of the water balance. Environ. Res. Lett. 14 (5), 055005. https://doi.org/10.1088/1748-9326/ab1049.